Seasonal observations of carbonate chemistry and ocean acidification in 2010

Prepared for

ConocoPhillips Company
P.O. Box 100360
Anchorage, AK 99510-0360

Shell Exploration & Production Company
3601 C Street, Suite 1334
Anchorage, AK 99503

and

Statoil USA E & P, Inc
2700 Gambell St
Anchorage, AK 99507

Final Report

Prepared by:

Jeremy T. Mathis
Assistant Professor
Chemical Oceanography
University of Alaska Fairbanks
School of Fisheries and Ocean Sciences
245 O'Neill BLDG
Fairbanks, AK 99775-7220
Phone: (907) 474-5926
jmathis@sfos.uaf.edu

December 2011

Executive Summary

Samples were collected and analyzed for dissolved inorganic carbon and total alkalinity in August, September, and October in the Berger, Klondike, and Statoil lease sites in the eastern Chukchi Sea. These samples where used to calculate the pH, partial pressure of CO_2, and carbonate mineral saturation states for calcite and aragonite in the water column. The data was consistent with recent studies in the region that showed that phytoplankton primary production in late spring significantly alters the carbon biogeochemistry of the water column throughout the year. Early in the ice-free period, primary production consumes DIC in the euphotic zone causing pH and carbonate mineral saturation states to increase. However, much of the organic matter that is produced is exported from the surface making the eastern Chukchi Sea a strong sink for atmospheric CO_2. As the organic matter settles near the bottom and is broken down by bacteria, DIC concentrations increase sharply, particularly later in the year, driving down pH and suppressing the concentrations of important carbonate minerals that are necessary for shell growth in benthic calcifying organisms. The data from 2010 shows a definitive seasonal progression of this process with aragonite becoming partially undersaturated along the bottom in September, and broadly undersaturated in October. While carbonate saturation states would naturally be suppressed by the high rates of export production, the penetration of anthropogenic CO_2 into water column (ocean acidification) has caused the observed undersaturations and these will likely expand as CO_2 levels in the atmosphere continue to rise in the coming decades. It is unclear at this time what the implications to the benthic calcifying ecosystem will be due to ocean acidification.

Table of Contents

Introduction

The Arctic Ocean plays an important and likely increasing role in both the regional and global climate system with complex and poorly constrained interactions and feedbacks between sea-ice, the ocean and atmosphere and the hydrological cycle. Some of these interactions have a significant impact on the global balance and atmospheric concentrations of greenhouse gases such as carbon dioxide (CO_2). Currently, the Arctic basin is an important sink for atmospheric CO_2 with recent estimates suggesting that the region contributes between 5 to 14% to the global ocean's net uptake of CO_2 (Bates and Mathis, 2009). In the lease sites being studied here, the Chukchi Sea is a strong seasonal sink for atmospheric CO_2.

The uptake of CO_2 by the Arctic Ocean is of particular importance because since the Industrial Revolution the oceans have absorbed approximately 127 Pg (Pg =1015 g C) of anthropogenically produced CO_2 from the atmosphere (Sabine and Feely, 2007). While this has mitigated the increase in atmospheric CO_2 concentrations by ~55% (Sabine et al., 2004; Sabine and Feely, 2007), it has changed the carbonate chemistry of seawater chemical speciation (e.g., Caldiera and Wickett, 2003; Andersson and Mackenzie, 2004; Feely et al., 2004; Orr et al., 2005; Millero, 2007) with unknown, but potentially significant impacts to current and future marine ecosystems (Fabry et al., 2008, 2009; Cooley and Doney, 2009). The absorption of atmospheric CO_2 by the ocean has resulted in a lowering of pH, especially over the last few decades (e.g., Bates, 2007; Byrne et al., 2010) as atmospheric CO_2 levels have risen sharply, with a subsequent decrease in the availability of carbonate ions (CO_3^{2-}) and a suppression of the saturation states (Ω) of calcium carbonate minerals ($CaCO_3$), which could result in a reduction of suitable habitat for marine calcifiers. These processes, collectively termed "ocean acidification" (OA), have occurred naturally over geologic time scales (e.g. Zachos et al., 2005) but have been accelerated due to anthropogenic emissions from industrial processes and changes in land use (Feely et al., 2004; Sabine et al. 2004; Orr et al., 2005; Caldiera and Wickett, 2005).

Because of these rapid environmental changes, the Arctic marine carbon cycle will likely enter a transition period in the coming decades, with large uncertainties in the exchange of atmosphere-ocean CO_2 (Anderson and Kaltin, 2001; Bates et al., 2006; Bates and Mathis, 2009; Cai et al., 2010; Jutterstrom and Anderson, 2010) in response to sea-ice loss and other climate-change induced processes, such as warming temperatures and changes in primary production.

Furthermore, the Arctic marine carbon cycle and marine ecosystems are also vulnerable to ocean acidification that results from the uptake of anthropogenic CO_2 from the atmosphere (Orr et al., 2005; Steinacher et al., 2009; Bates et al., 2009; Yamamoto-Kawai et al., 2009).

Background

The Arctic Ocean occupies ~2.6% of the surface area of the global ocean, but contains <1% of the total ocean volume. It is a Mediterranean type sea that is almost completely surrounded by landmasses, with only few communication points with other ocean basins. Given its geographical layout, it is disproportionately impacted by terrestrial fluxes and receives almost 10% of the total global river runoff annually from an extensive system of rivers and smaller coastal streams that drain the watersheds of Siberia and northern North America (McGuire et al., 2006; Cooper et al., 2008). However, these discharges are episodic, with the majority of the total flux occurring in late spring and summer. The landmasses surrounding the Arctic basin contain large stores of terrestrial carbon and strongly influence the biogeochemical dynamics of the marine carbon cycle.

For half the year, the Arctic Ocean is almost completely covered by sea-ice with only small areas of open water in the form polynyas and flaw-leads. This seasonal sea-ice cover plays a major role in controlling the carbon cycle through vertical homogenization of the water-column by physical processes such as ventilation, brine rejection and convective mixing. In the western Arctic (i.e. Chukchi Sea), seasonal atmospheric warming and the inflow of warm, lower salinity waters from Pacific sources leave the broad Chukchi shelf nearly sea-ice free for most of the summer months.

The wide and shallow Chukchi Sea occupies a particularly extensive portion of the western Arctic Ocean. Relatively warm and nutrient-rich Pacific Ocean waters enter the Chukchi Sea, flowing northward through Bering Strait from the Bering Sea (Coachman et al., 1975; Roach et al., 1975; Woodgate et al., 2005). As such, the physics and carbon biogeochemistry of the Chukchi Sea is highly influenced by this inflow and can be characterized as an "inflow" shelf (Carmack and Wassmann, 2006; Bates and Mathis, 2009).

Inflow of Pacific Ocean water through Bering Strait into the Chukchi Sea delivers ~0.8-1.0 Pg C $year^{-1}$ of inorganic carbon into the Arctic Ocean (Bates and Mathis, 2009), with outflow from the western Arctic primarily through the Canadian Archipelago. In comparison, rates of primary production from marine phytoplankton and ice algae have been determined to be ~135 Tg C yr^{-1} (Tg = 10^{12} g) in the entire Arctic Ocean, although there are large uncertainties in these estimates (Macdonald *et al*., 2010). The Arctic landmasses contain even larger stores of carbon compared to the marine environment, and there are significant river inputs of organic carbon to the Arctic shelves (e.g., Lobbes et al., 2000; Amon, 2004; Rachold et al., 2004; Guo and Macdonald, 2006; Raymond et al., 2007; Holmes et al., 2011). Pan-arctic river inputs of carbon have been estimated by McGuire et al. (2009) at 33 Tg C yr^{-1} of DOC and 43.2 Tg C yr^{-1} DIC, which are 7.1% and 10.6% of their respective total global total river fluxes (Cai et al., 2011). River inputs of particulate organic carbon (POC) and coastal erosion of terrestrial carbon (mostly refractory organic carbon) have also been estimated at ~12 Tg C yr^{-1} (e.g., Rachold et al., 2004; Macdonald et al., 2009). Arctic rivers thus contribute disproportionately large amounts of carbon to the Arctic Ocean compared to other ocean basins.

Compared to many other open-ocean and coastal environments, relatively few studies of the marine carbon cycle have been conducted in the western Arctic. The harsh polar climate and difficult logistical support have limited most studies to opportunistic icebreaker surveys conducted on the Arctic Ocean shelves during the summertime sea-ice retreat. Even with large-scale, multiyear projects such as the Shelf-Basin Interactions (SBI II) (Grebmeier et al., 2008), spring and summer observations of the Arctic Ocean marine carbon cycle are highly limited and virtually absent during fall and winter. Thus, there are considerable uncertainties about the physical and biological controls on the marine carbon cycle, natural and human perturbed seasonal and interannual variability, CO_2 sinks and sources in the Arctic Ocean and ocean acidification.

Biological Production

The inflow of nutrient-rich water from the Pacific Ocean into the Chukchi Sea (Codispoti *et al*., 2005), coupled with near constant light in summer supports a brief, but intensive period of marine phytoplankton photosynthesis and growth compared to other Arctic Ocean shelves (Cota

et al., 1996; Hill and Cota, 2005) where nutrients are more limited. Occupying the base of the food web, phytoplankton primary production rates on the Chukchi Sea shelf can exceed ≥300 g C m^2 y^{-1} or 0.3-2.8 g C m^2 d^{-1} (e.g., Hameedi, 1978; Cota et al., 1996; Gosselin et al., 1997; Hill and Cota, 2005; Bates et al., 2005a; Mathis et al., 2009; Macdonald et al., 2009). Intense seasonal growth of marine phytoplankton supports a large zooplankton (e.g., copepods; see Hopcroft report for description in the study area) biomass that in turn supports diverse open-water and seafloor ecosystems (Feder et al., 2005; Grebmeier et al., 2008). Both pelagic and benthic ecosystems on the Chukchi Sea shelf support marine mammal (e.g., grey whale, walrus, polar bears), seabird and human populations in the region.

In the Chukchi Sea, the brief period of high rates of marine phytoplankton primary production results in the formation of high concentrations of suspended particulate organic carbon (sPOC) (Bates *et al*., 2005b; Moran et al., 2005; Lepore et al., 2007) (**Figure 1**). High concentrations of sPOC have been observed (up to 2000 mg C L^{-1}; average of ~200-300 mg C L^{-1}) across the shelf, with considerable export of sPOC off the shelf into the Canada Basin (Bates et al., 2005b), and relatively high rates of vertical export of organic carbon to shelf, slope and basin sediments (Moran et al., 2005; Lepore et al., 2007). The ecosystem is dominated by large sized phytoplankton (Grebmeier et al., 2008) that produce a relatively large size class of organic matter (i.e., as POC) that is rapidly exported to the bottom waters over the shelf.

Air-Sea Fluxes of CO_2

The export character of the shelf is what conditions the surface waters of the Chukchi Sea to be a strong sink for atmospheric CO_2. Early studies of the Chukchi Sea (Semiletov1999) showed that seawater pCO_2 (~200-350 µatm) values were lower than the atmosphere (~365-380 µatm at the time of observation) during the sea-ice free period. Since then, other studies have observed similarly low seawater pCO_2 conditions on the Chukchi Sea shelf during summertime (~150-350 µatm; Pipko et al., 2002; Murata and Takizawa, 2003; Bates et al., 2005a; 2006; Bates, 2006; Chen and Gao, 2007; Fransson et al., 2009; Andreev et al., 2009). Large drawdowns of surface water DIC from primary production is the primary controller of pCO_2 values in summer (Bates et al., 2005; Bates, 2006; Cai et al., 2010). The seasonal changes in DIC have been largely attributed to high rates of summertime phytoplankton primary production or

net community production (Bates *et al*., 2005; Mathis *et al*., 2007a), especially in the vicinity of Barrow Canyon (at the northern edge of the Chukchi Sea shelf; Bates et al., 2005a; Hill and Cota, 2005) which is close to the lease areas. However, the seasonal decrease in pCO_2 values is somewhat moderated by warming temperatures that drive pCO_2 values higher. The seasonal rebound of seawater pCO_2 and DIC during wintertime likely results from the uptake of CO_2 from the atmosphere and winter mixing induced from brine rejection (Anderson et al., 2004; Omar et al., 2005).

Early season observations in the Chukchi Sea indicate that these processes return the surface waters to near saturation compared to atmospheric pCO_2 values before ice retreat and the onset of the spring bloom. After the bloom, summertime pCO_2 values are typically in the range of –50 to -200 μatm relative to the atmosphere, creating a strong driving force for air-sea exchange. Previous estimates of the rates of air-sea CO_2 exchange during the sea-ice free period in the summertime have ranged from ~-20 to -90 mmol CO_2 m^{-2} d^{-1} (Wang et al., 2003; Murata and Takizawa, 2003; Bates, 2006; Fransson et al., 2009) indicating that the surface waters of the Chukchi Sea shelf have the potential to be a strong sink of atmospheric CO_2 (Kaltin and Anderson, 2005). The annual ocean CO_2 uptake for the Chukchi Sea shelf has been estimated at 2-9 mmol C m^{-2} y^{-1} (Katlin and Anderson, 2005; Bates, 2006), or approximately11 to 53 Tg C yr^{-1}. These studies show that the Chukchi Sea shelf dominates air-sea CO_2 fluxes in the western Arctic region.

Ocean Acidification

The drawdown of DIC during the spring phytoplankton bloom has a significant impact on water column pH and the saturation states of the two most important carbonate minerals (calcite and aragonite). As DIC is consumed, pCO_2 drops in the surface layer causing pH to increase, raising the saturation states of calcite and aragonite. In response to high export production, the remineralization of organic matter increases the concentration of DIC and pCO_2 in bottom waters and suppresses carbonate mineral saturation states to a varying degree across the Chukchi shelf. In the region near the head of Barrow Canyon, export production is highest and this is where the strongest seasonal suppression of aragonite in subsurface water has been observed. This suppression of carbonate mineral saturation states corresponds to high apparent oxygen

utilization (AOU) rates and elevated silicate in the bottom waters indicating both pelagic and benthic remineralization. The subsurface effects of remineralization can be especially significant during periods of intense production when saturation states increases at the surface. These biologically driven, seasonally divergent trajectories of Ω, or the "Phytoplankton-Carbonate Saturation State" (PhyCaSS) Interaction, have been observed in the Chukchi Sea (Bates *et al.*, 2009; Bates and Mathis, 2009), and are likely typical of highly productive polar and sub-polar shelves.

The PhyCaSS Interaction could be particularly influential on benthic calcifiers in the Chukchi Sea because the lowest saturation states coincide with areas of highest export production. It appears that the export production, which provides the food source at the bottom, is causing the undersaturation that could inhibit shell and test growth in calcifying organisms. This PhyCass interaction is now being exacerbated by the penetration of anthropogenic CO_2 into the oceans, particularly in high latitude regions.

The decrease in seawater pH due to the uptake of anthropogenic CO_2 (Bindoff et al., 2007; Bates, 2007) has been termed "ocean acidification" and has been observed at several open-ocean time-series locations (e.g. Bermuda Atlantic Time Series (BATS) and the Hawaii Ocean Time Series (HOTS)). The uptake of anthropogenic CO_2 has already decreased surface water pH by 0.1 units when averaged across the global ocean. IPCC scenarios, based on present-day CO_2 emissions, predict a further decrease in seawater pH by 0.3 to 0.5 units over the next century and beyond (Caldeira and Wickett, 2003). Ocean acidification and decreased pH reduces the saturation states of calcium carbonate minerals such as aragonite and calcite, with many studies showing decreased $CaCO_3$ production by calcifying fauna (Buddemeier et al., 2004; Fabry et al., 2008) and increased $CaCO_3$ dissolution. The Arctic Ocean is particularly vulnerable to ocean acidification due to relatively low pH and low temperature of polar waters compared to other waters (Orr et al., 2005; Steinacher et al., 2009) and low buffer capacity of sea-ice melt waters (Yamamoto-Kawai et al., 2009).

In the Arctic Ocean, potentially corrosive waters are found in the subsurface layer of the central basin (Jutterstrom and Anderson, 2004; Yamamoto-Kawai et al., 2009; Cheirici and Fransson, 2009), on the Chukchi Sea shelf (Bates et al., 2009) and in outflow waters of the Arctic found on the Canadian Arctic Archipelago shelf (Azetsu-Scott et al., 2010). On the

Chukchi Sea, waters corrosive to $CaCO_3$ occur seasonally in the bottom waters with unknown impacts to benthic organisms.

As described above, the seasonally high rates of summertime phytoplankton primary production in the Chukchi Sea drives a downward export of organic carbon, which is remineralized back to CO_2 which in turn increases seawater pCO_2 (and decreasing pH) of subsurface waters. Such a seasonal biological influence on the pH of subsurface waters amplifies existing impacts of ocean acidification induced by the uptake of anthropogenic CO_2 over the last century (Bates et al., 2009). Given the scenarios for pH changes in the Arctic, the Arctic Ocean and adjacent Arctic shelves including the western Arctic, will be increasingly affected by ocean acidification, with potentially negative implications for shelled benthic organisms as well as those animals that rely on the shelf seafloor ecosystem.

Methods

Cruise Information and Water Column Sampling

Physical, chemical and biological measurements were made during cruises to the study area in August, September, and October of 2010 (**Figure 2**). Samples for dissolved inorganic carbon (DIC) and total alkalinity (TA) were collected at all three studies sites in August and September and only at the Burger Site in October. Seawater samples for DIC/TA were drawn from Niskin bottles into pre-cleaned ~300 mL borosilicate bottles. These samples were subsequently poisoned with mercuric chloride ($HgCl_2$) to halt biological activity, sealed, and returned to the laboratory for analysis. All sampling and analysis was performed in compliance with the guide to best practices for ocean acidification research and reporting (Riebesell *et al.*, 2010).

Laboratory Analysis and Calculation of Carbonate Parameters

DIC and TA samples were analyzed using a highly precise and accurate gas extraction/coulometric detection system (Bates, 2001). The analytical system consists of a VINDTA 3C (Versatile Instrument for the Detection of Total Alkalinity; http://www.marianda.com) coupled to a CO_2 coulometer (model 5012; UIC Coulometrics). TA samples were also determined by potentiometric titration using the VINDTA 3C. Routine

analyses of Certified Reference Materials (CRMs, provided by A.G. Dickson, Scripps Institution of Oceanography) ensured that the accuracy of the DIC and TA measurements were within 0.05% (~1 μmoles kg^{-1}) and stable over time.

Seawater pCO_2, pH and $CaCO_3$ saturation states for calcite ($\Omega_{calcite}$) and aragonite ($\Omega_{aragonite}$) were calculated from DIC, TA, temperature, salinity, phosphate, and silicate data using the thermodynamic model of Lewis and Wallace [1995]. The carbonic acid dissociation constants of Mehrbach *et al*. (1973) [refit by (Dickson and Millero, 1987); i.e., pK_1 and pK_2] were used to determine the carbonate parameters. The CO_2 solubility equations of Weiss (1974), and dissociation constants for borate (Dickson, 1990), silicate and phosphate (Dickson and Goyet, 1994) were used as part of the calculations. Uncertainty in the calculation of $\Omega_{calcite}$ and $\Omega_{aragonite}$ were ~0.02.

Basis of the Arctic Marine Carbonate System

As CO_2 levels rise in the atmosphere, the increased partial pressure of carbon dioxide (pCO_2) in seawater contributes to OA and the suppression of biologically important carbonate mineral concentrations, such as calcite and aragonite, through a series of well-known reactions:

$$CO_{2(g)} \leftrightarrow CO_{2(aq)} \quad (1)$$

$$CO_{2(aq)} + H_2O \leftrightarrow H_2CO_3 \quad (2)$$

$$H_2CO_3 \leftrightarrow H^+ + HCO_3^- \quad (3)$$

$$H^+ + HCO_3^- \leftrightarrow 2H^+ + CO_3^{2-} \quad (4)$$

$$CO_3^{2-} + Ca^{2+} \leftrightarrow CaCO_3(s) \quad (5)$$

Following dissolution (Eq. 1), dissolved CO_2 undergoes hydration reactions to form carbonic acid (Eq. 2), which rapidly dissociates to form carbonate and releases hydrogen ions (Eqs. 3, 4). Almost all of the produced carbonate ions react with calcium to form mineral solids (Eq. 5), preventing this reaction from contributing to dissolved alkalinity. Further, most of the free hydrogen ions produced react with the naturally dissolved alkalinity in seawater, reducing

carbonate ion concentrations. The remaining hydrogen ions contribute to the lowering of pH. Carbonate mineral saturation states are dependent on the concentration of free carbonate ions according to the following equations, such that a reduction in available CO_3^{2-} (Eq. 5) decreases the saturation states of both aragonite and calcite:

$$\Omega_{aragonite} = \frac{[Ca^{2+}][CO_3^{2-}]}{K^*_{sp_{aragonite}}} \quad (7)$$

$$\Omega_{calcite} = \frac{[Ca^{2+}][CO_3^{2-}]}{K^*_{sp_{calcite}}} \quad (8)$$

Cold ocean temperatures increase the solubility of CO_2 and precondition the seawater to have lower calcium carbonate concentrations and saturation states compared to more temperate ocean environments, leaving polar and sub-polar shelves particularly vulnerable to OA (Orr *et al.*, 2005; Bates and Mathis, 2009; Fabry *et al*., 2009; Steinacher *et al.*, 2009). In addition to this temperature effect, several other processes affect the carbonate system and can contribute to the intensification of OA in polar and subpolar regions, including seasonally high rates of primary production, river runoff, and sea-ice formation and melt processes (e.g. Bates and Mathis, 2009; Bates et al., 2009). For example, seasonally intense periods of primary production are uncoupled from grazing in most polar environments (e.g., Springer *et al.*, 1996; Macdonald *et al.*, 2009) leading to high rates of organic matter export from the surface layer (e.g. Mathis et al., 2007). While this export production supports the biologically diverse benthic communities in these regions it leads to elevated rates of remineralization in bottom waters and sediments. Thus, ocean biology tends to drive seasonally divergent trajectories for seawater chemistry, with primary production in the euphotic zone increasing Ω in the mixed layer while an accumulation of DIC in subsurface waters through remineralization suppresses Ω (e.g. Bates et al., 2009). The reduction and undersaturation of carbonate minerals, particularly in bottom waters of polar and subpolar seas could have implications for benthic ecosystems. Further decreases in pH and Ω could have significant consequences for the benthic and pelagic ecosystems in a region where organisms are already struggling to adapt to changing environmental conditions (Løvvorn *et al.*, 2003; Moore *et al.*, 2003; Overland and Stabeno, 2004; Grebmeier *et al.*, 2006).

Results

1002 – The August Cruise

The most intense period of phytoplankton primary production had already occurred when the study area was occupied for the first time in August of 2011 (**Figure 2**). DIC concentrations that had been drawn down in the mixed layer by the bloom were likely already starting to increase due to air-sea exchange of CO_2. Nutrients, particularly nitrate was very low in the mixed layer meaning there was very little potential for any new primary production to occur, although there is always some secondary production due to nitrogen uptake from other sources such as ammonia.

Observations from the first occupation (1002) in the three lease sites showed that DIC was coupled to salinity (**Figure 3**), with concentration ranging from ~2200 µmoles kg^{-1} near the bottom (salinity of 33.5) to a minimum value of ~1800 µmoles kg^{-1} in surface waters (salinity of 28.5) (**Tables 1, 2 and 3**). There was an apparent accumulation of DIC in the bottom waters (salinity 32.5 – 33.5) of the shelf likely in response to the remineralization of exported organic matter. TA exhibited an even tighter correlation with salinity (Figure 4). Minimum values of TA (~2000 µmoles kg^{-1}) were observed in the surface waters and concentrations increased with depth to a maximum of 2280 µmoles kg^{-1} near the bottom (salinity of 33.5).

As discussed earlier, the removal of DIC from the surface layer by primary producers in late spring and summer causes a sharp decrease in the partial pressure of CO_2 (pCO_2) in the mixed layer. Although several months had passed since the bloom during the August occupation there were still considerable pCO_2 undersaturations relative to atmospheric values (385µatm) (**Tables 1, 2 and 3**). In the surface layer, pCO_2 values ranged from ~180 µatm to ~320 µatm (**Figure 5**), indicating that the surface waters still had a great deal of potential to take up CO_2 from the atmosphere. The differences in pCO_2 at the surface are a function of biological production (some areas are more nutrient rich and allow for greater drawdown of DIC) during the spring and summer. In the deeper waters, particularly below the well-stratified surface layer, pCO_2 values increased sharply to >400 µatm in response to the DIC accumulation from remineralization (**Figure 5; Tables 1, 2, and 3**).

The consumption of DIC strongly influenced pH, lowering values in the surface layer (**Figure 6**) after the bloom. pH values in August were still higher (less acidic) than "pre-bloom values" (observed during other studies in the region during the pre-ice melt spring of 2010) ranging from ~8.05 – 8.32 at the surface (**Tables 1, 2, and 3**). However, the increased pCO_2 at depth caused pH to be much lower with most of the values falling between 8.0 and 8.1 (**Figure 6**).

The changes in DIC concentrations at the surface and at the bottom had a profound effect on the carbonate mineral saturation states (**Figures 7 and 8**). Both calcite and aragonite were supersaturated throughout the water column in August, but there was a clear gradient between the surface and the bottom. Calcite values ranged from ~2.5 – 3.6 at the surface (**Tables 1, 2, and 3**), with the minimum values (~1.6) occurring in the bottom waters. Aragonite showed a similar trend, with values overall being lower than calcite, but this is due to the greater solubility of aragonite in seawater. Aragonite values approached the saturation horizon ($\Omega = 1.0$) near the bottom, but remained above this threshold in August (**Figure 8**; **Tables 1, 2 and 3**).

There were some spatial differences in the carbonate parameters in the surface waters during August (**Figure 9**), but generally they were fairly uniform. DIC concentrations were lower in the northern and western regions of the study area as was TA. This is likely due to the presence of lower salinity water from ice-melt, which is low in DIC and TA concentrations. The remaining carbonate parameters exhibited a similar trend as they are largely controlled by DIC and TA concentrations (**Figure 9**). pCO_2 was highly undersaturated at the surface (**Tables 1, 2 and 3**) relative to the atmosphere (385 μatm) and the region was a strong sink for atmospheric CO_2, which is consistent with other studies in the region.

The distribution of DIC and TA were much more uniform at the bottom of the study (**Figure 10; Tables 1, 2 and 3**) in August compared to the surface. DIC and TA concentrations were ~2150 and 2250 μmoles kg^{-1}, respectively, but did show a slight gradient with concentrations of both parameters increasing northward. This is likely do to both increased export production as the water naturally moves northward and a greater influence of higher salinity water from the shelf break, which would have contained higher concentrations of TA. pCO_2 in the bottom waters were at or above atmospheric concentrations. The pH of the bottom

waters was close to 8.0 and as discussed above, the saturation states for calcite and aragonite were all above 1.0 (**Tables 1, 2, and 3**).

1003 – The September Cruise

During the September cruise, DIC concentrations in the surface layer were higher than those observed in August (**Tables 4, 5 and 6**), and were again fairly well correlated with salinity (**Figure 3**). This seasonal increase in DIC concentrations is due to the uptake of CO_2 from the atmosphere. DIC concentrations in the bottom waters (salinity of 33.5) also increased significantly compared to August values (**Tables 4, 5 and 6**). This is clear evidence of the impact that the remineralization of organic matter has on DIC concentrations along the bottom. TA also increased compared to August values (**Tables 4, 5 and 6)** and maintained a tight correlation with salinity (**Figure 4**). It has been shown that storm systems in fall can induce upwelling along the shelf break and bring higher salinity water with elevated concentrations of DIC and TA onto the shelf, which could also explain some of the seasonal increase.

The increase in DIC concentrations at the surface is likely a product of the uptake of CO_2 from the atmosphere, although a small part of the this increase is likely due to remineralization of dissolved organic carbon (DOC) in the surface layer or suspended particles that were too light to sink. The combinations of these two processes caused pCO_2 at the surface to increase significantly (**Tables 4, 5, and 6**) and at some locations the water became supersaturated with respect to atmospheric CO_2 (**Figure 5**). In fact, the highest pCO_2 values observed during all three cruises occurred during September. Near the bottom, pCO_2 values also increased sharply compared to August observations (**Tables 4, 5, and 6**), and in some locations exceeded 600 μatm (**Figure 5**).

pH and the saturation states of calcite and aragonite responded to these changes in pCO_2 at the surface and near the bottom (**Figures 6, 7, and 8**). pH values were the lowest observed (8.0) during this time at the surface. Both calcite and aragonite decreased (**Tables 4, 5, and 6**), but both remained well above the saturation horizon at the surface (**Figures 7 and 8**). The accumulation of DIC at depth and the subsequent increase in pCO_2 caused the saturation states to drop sharply near the bottom with aragonite becoming undersaturated ($\Omega < 1.0$) in a few locations (**Figure 8**), although calcite remained above the saturation horizon (**Figure 7**).

Spatially, DIC and TA concentrations were less uniform compared to August (**Figure 11**). In the northeastern section of the study area there was a low DIC/TA feature present in September, likely due to river runoff and ice-melt. This caused pCO_2 to be lower at these locations and pH and carbonate mineral saturation states to be higher. Near the bottom, the increase in DIC concentrations compared to August was obvious (**Figure 12**) as were the higher values of pCO_2 in the southwestern part of the study area. This increase in pCO_2 seems to be related to an increase in temperature along the bottom in that region. The lowest saturation states for calcite and aragonite can also been seen in this area.

1004 – The October Cruise

Although the October cruise was limited to only the Burger site, a number of important observations were made showing the continuation of the seasonal progressions that drives the carbonate system in the Chukchi Sea. Observations of DIC showed a divergence from salinity (**Figure 3**), particularly in the upper 30 m concentrations were drawn down by >150 μmoles kg^{-1} in some locations (**Figure 3**). However, in the surface waters, concentrations increased significantly between September and October (**Table 6**). There is also evidence of increased TA concentrations (salinity of ~29.75), which only could have come from deeper, offshore waters. Although this feature needs additional synthesis effort, I believe that an upwelling event brought nutrient-rich water into the mixed layer and stimulated a "late-season" bloom, which consumed DIC at some stations, while air-sea exchange added DIC in other locations causing the divergent trajectory observed in **Figure 3** (salinity range between 29.5 and 30). One of these processes would have been dominant in each location, leading some stations to exhibit an increase in DIC, while others showed a decrease. It has long been hypothesized that these late blooms occur and may account for a significant part of the total annual productivity in the Chukchi Sea, but direct observations have been absent. The data here clearly warrants further study.

In response to the drawdown of DIC and decreasing temperatures, pCO_2 exhibited some of the lowest values (**Figure 5**) in October again illustrating the strong potential sink for atmospheric CO_2 that the Chukchi Sea provides. pCO_2 values near the bottom increased sharply (**Table 6**) compared to September, and particularly August as the remineralization loop continued to add DIC to the water column. pCO_2 was above 500 μatm at most locations and

exceeded 600 µatm at some stations (**Table 1**). The increase in pCO_2 caused pH to drop below 7.9 at most locations below mixed layer (**Figure 6**). This induced broad undersaturations for aragonite from 30 m to the bottom over most of the study area (**Figure 8**). Calcite values remained supersaturated, but did show a seasonal decrease of almost 1.5 units from August to September. The sink potential for atmospheric CO_2 at the surface and the persistent undersaturations for aragonite are apparent in **Figures 13 and 14,** respectively**.**

Discussion

As noted above, there were a number of changes in the carbonate system throughout the water column from August to October. In August, surface waters at the Klondike site (**Figure 15**) showed a strong longitudinal gradient from west to east. On the western side, salinity, DIC and TA were considerably lower than on the eastern side. However, temperatures were warmer on the eastern side. This low salinity, low temperature feature was likely ice-melt, sitting over that portion of the shelf. The low DIC and TA concentrations in this water, which are indicative of ice-melt, caused pH to be as high as 8.3. Aragonite was supersaturated throughout the surface layer, but was higher on the western side. Salinity, DIC, and TA were much more uniform across the bottom with DIC and TA concentrations being ~2100 and ~2200 µmoles kg^{-1}, respectively below ~25 m. pH ranged between 8.0 and 8.1, while aragonite saturation states were ~1.5.

In September, the low salinity feature on the western side of the Klondike site was absence and values for DIC and TA were uniform (~2000 and 2150 µmoles kg^{-1}, respectively) in the surface waters in the highly stratified water column (**Figure 16**). Temperatures at the surface and near the bottom had increased between August and September, which lead to some of the increases in pCO_2 values discussed earlier. pH values ranged between 8.0 and 8.1 and aragonite saturation states were between 1.5 and 2.0 in the upper 20 m of the water column. Along the bottom, DIC and TA concentrations were ~2100 and ~2200 µmoles kg^{-1}, respectively. pH and aragonite saturation states were ~8.0 and ~1.5 below 25 m.

Observations in August at the Burger (**Figure 17**) site showed the same low salinity feature on the western side of the study area that was present at Klondike, with subsequently low DIC and TA values. This was also likely due to ice-melt. pH was ~8.3 in this feature and

aragonite saturation states were between 1.5 and 2.0. Below the surface layer, concentrations of DIC and TA were fairly constant as was temperature and salinity.

The occupation of the Burger site in September showed that the low salinity feature was gone and the water column had horizontally stratified with only a small, lower salinity/temperature feature present around 165.25°W (**Figure 18**). Concentrations of DIC and TA were also stratified and increased with depth, with values at the surface and near the bottom higher than in August. The saturation state for aragonite was still >1.5 in the upper 20 m, but in the bottom water a decrease was apparent due to the increase in DIC concentrations.

Observations at the Berger site in October (**Figure 19**) showed some definitive differences compared to earlier months. Temperature and salinity profiles showed that the water column was still relatively horizontally stratified. However, concentrations of DIC and TA had decreased <1900 and <2100 μmoles kg^{-1}, respectively in the upper 20 m. DIC had increased in the bottom waters to around 2200 μmoles kg^{-1}. This increase in DIC concentrations caused pH values to drop below 7.9 and aragonite to become highly ($\Omega_{arg} < 0.8$) undersaturated.

In the Statoil area, observations in August (**Figure 20**) showed the water column was horizontally stratified with a small east-west gradient in salinity and temperature, likely from the influence of the Alaska Coastal Current (ACC) on the eastern side of the study area. DIC and TA concentrations showed a similar trend with values being lower in the surface waters on the eastern side. Both pH and aragonite saturation states were higher in these locations.

In September (**Figure 21)**, that water column at the Statoil site remained highly stratified, but there was still some evidence of ACC water closer to the coast, where pH and aragonite saturation states were slightly higher. However, the bottom waters in this area showed the influence of the increase in DIC concentrations and aragonite saturation states were near undersaturation.

The Impact of Anthropogenic CO_2

Ideally, the amount of anthropogenic CO_2 in a given system can be estimated by directly calculating the age of the water mass, but a paucity of data in this region prevents this approach. However, based on the origin of the water on the Chukchi Sea shelf and the observed density constraints, we can approximate anthropogenic CO_2 inventories to evaluate the pre-industrial

state of the carbon cycle in the region. Sabine *et al.* (2004) estimated that ~ 35 μmoles kg^{-1} anthropogenic CO_2 has penetrated into waters of the North Pacific Ocean to the 26 kg m^{-3} isopycnal surface. Because the source waters of the western Arctic Ocean are derived from the Bering Sea Shelf/North Pacific a conservative assumption can be made that there is ~35 μmoles kg^{-1} of anthropogenic CO_2 in the water column of the Chukchi Sea.

To determine the impact of OA due to the uptake of anthropogenic CO_2, that 35 μmoles kg^{-1} can be subtracted from the DIC observations made during the cruises while keeping the remaining variables (TA, salinity, temperature) consistent with observations. The remaining carbonate parameters (specifically the saturation states for calcite and aragonite) can be recalculated using the thermodynamic model of Lewis and Wallace [1995]. When this was done for the 2010 data, the entire water column over the shelf was supersaturated with respect to aragonite during all three months and in all areas. While there are a number of weaknesses associated with this first order approximation, the calculation suggests that OA has resulted in the persistent aragonite undersaturations that have been observed in the Chukchi Sea. As atmospheric CO_2 concentrations increase, it is likely that these undersaturations will spread across the bottom waters of the shelf for at least parts of the year.

Timing of Ice Retreat

The timing of sea-ice retreat may also have a substantial effect on carbonate chemistry in subsurface waters. Ice retreat exerts a significant control on the fate of the organic matter produced during the phytoplankton blooms. Zooplankton grazing of seasonal production is minimal during blooms associated with colder surface water temperatures favoring the benthic ecosystem. In contrast, warmer years increase zooplankton production by up to 50%. Thus, colder waters are expected to be associated with higher export production to the benthos, and large remineralization signals will be generated at depth, corresponding to increases in pCO_2 and decreases in carbonate mineral saturation states. Warmer water blooms will retain carbon in the mixed layer and contribute to increased pelagic production and reduced bottom water remineralization.

Variation in the timing of sea-ice retreat could change the mode of production over the shelf. The earlier retreat of sea ice in recent years indicates that the blooms have been occurring

in colder water, favoring export production. If ice continues to retreat earlier in the spring it could lead to a dichotomy for benthic organisms. On the one hand, higher rates of export production should lead to increased food supply and an expansion of biomass. However, if high rates of export production coupled to increasing anthropogenic CO_2 inventories over the shelf cause expanded aragonite undersaturations it could lead to a reduction in habitat.

Concluding Remarks

The carbonate datasets collected during the 2010 surveys of the lease sites in the Chukchi Sea show the dynamic nature of the carbon cycle of the western Arctic Ocean. Brief, but intense periods of primary production in the surface layer in late spring sets the stage for most of the processes that occur for the remainder of the ice-free period. The consumption of DIC from phytoplankton dramatically lower the pCO_2 of the surface waters promoting broad regions of air-sea exchange and making the Chukchi Sea a strong sink for atmospheric CO_2. The removal of DIC also raises the pH and carbonate mineral saturation states, counteracting the effects of ocean acidification in the surface waters. However, the disconnects between phytoplankton primary production and zooplankton grazing causes large quantities of organic matter to be exported from the mixed layer. When this organic matter is remineralized by bacteria, it adds DIC back to the water column, lower pH and suppressing carbonate mineral saturation states near the bottom.

The Chukchi Sea has been productive for thousands of years and the remineralization of organic matter and the seasonal suppression of carbonate mineral saturation states is a natural phenomenon. However, the rising inventories of anthropogenic CO_2 in the water column has begun to drive saturation states past a threshold that will likely be detrimental to some marine calcifiers, particularly the diverse benthic organisms that dominates the Chukchi Sea. While ocean acidification is a global problem, the Arctic Ocean will likely experience the physical manifestations and potential impacts of it much sooner than more temperate regions and may be a bellwether for how the global ocean will respond. Over the last decade, numerous new datasets and insights have elucidated the complexities in the feedbacks of the Arctic carbon cycle, but they have also provided exciting new insights and enhanced our understanding of the region. It is critical that these investments in infrastructure and data gather efforts continue as the Arctic becomes open for more commercial development.

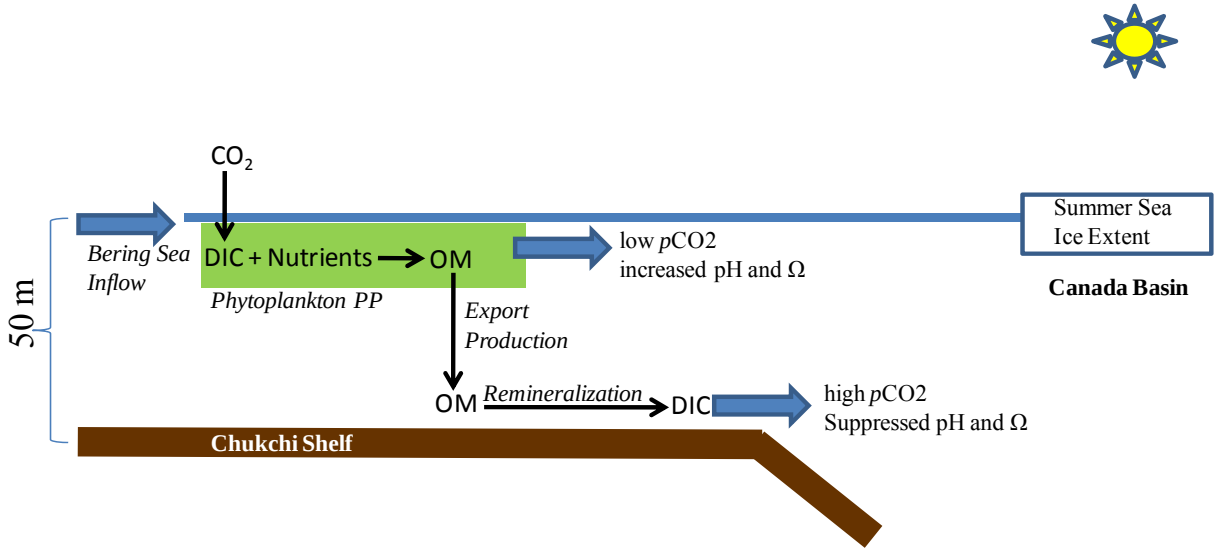

Figure 1 – Schematic of the influences on the carbon cycle in the Chukchi Sea. High rates of primary production (green box) consumes DIC, lowering the pCO_2 of the surface waters and promoting air-sea exchange. However, air-sea exchange happens much slower than primary production leaving the surface waters undersaturated with respect to atmospheric CO_2 for most of the summer. The removal of DIC from the surface water causes pH and carbonate mineral saturation states to increase. Due to limited grazing in the water column, most of the organic matter produced by the phytoplankton is exported to depth where it is remineralized back into DIC, increasing the pCO_2 of the bottom waters while lowering pH and suppressing carbonate mineral saturation states. Both the surface and bottom water masses are exported off of the Chukchi shelf conditioning the surface waters under the ice in the deep Canada Basin to be undersaturated with respect to atmospheric CO_2 and the upper halocline of the western Arctic Ocean to be undersaturated in aragonite.

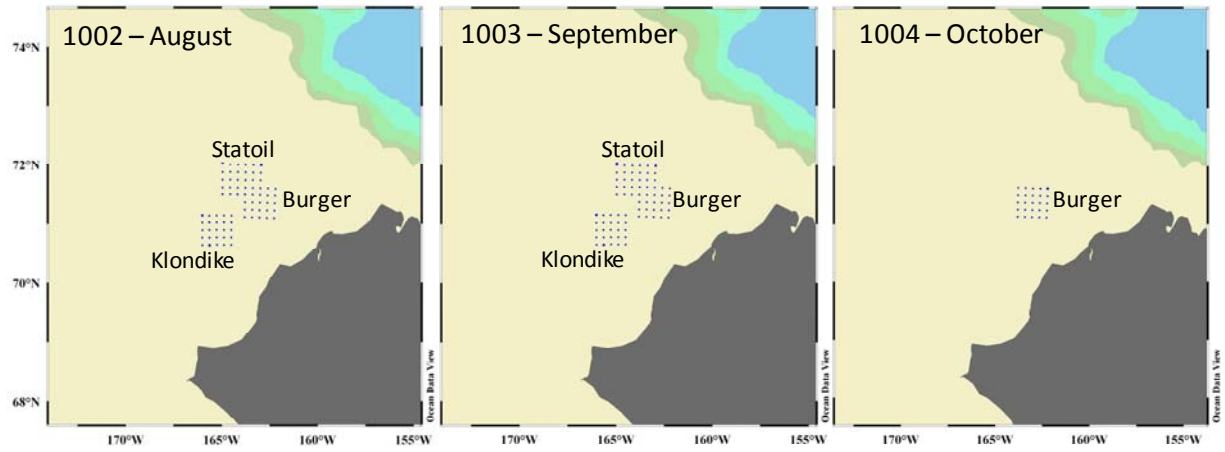

Figure 2 - Location of the study areas where carbon measurements were taken in 2010. Samples for DIC and TA were collected mostly at odd numbered stations in each of the lease areas.

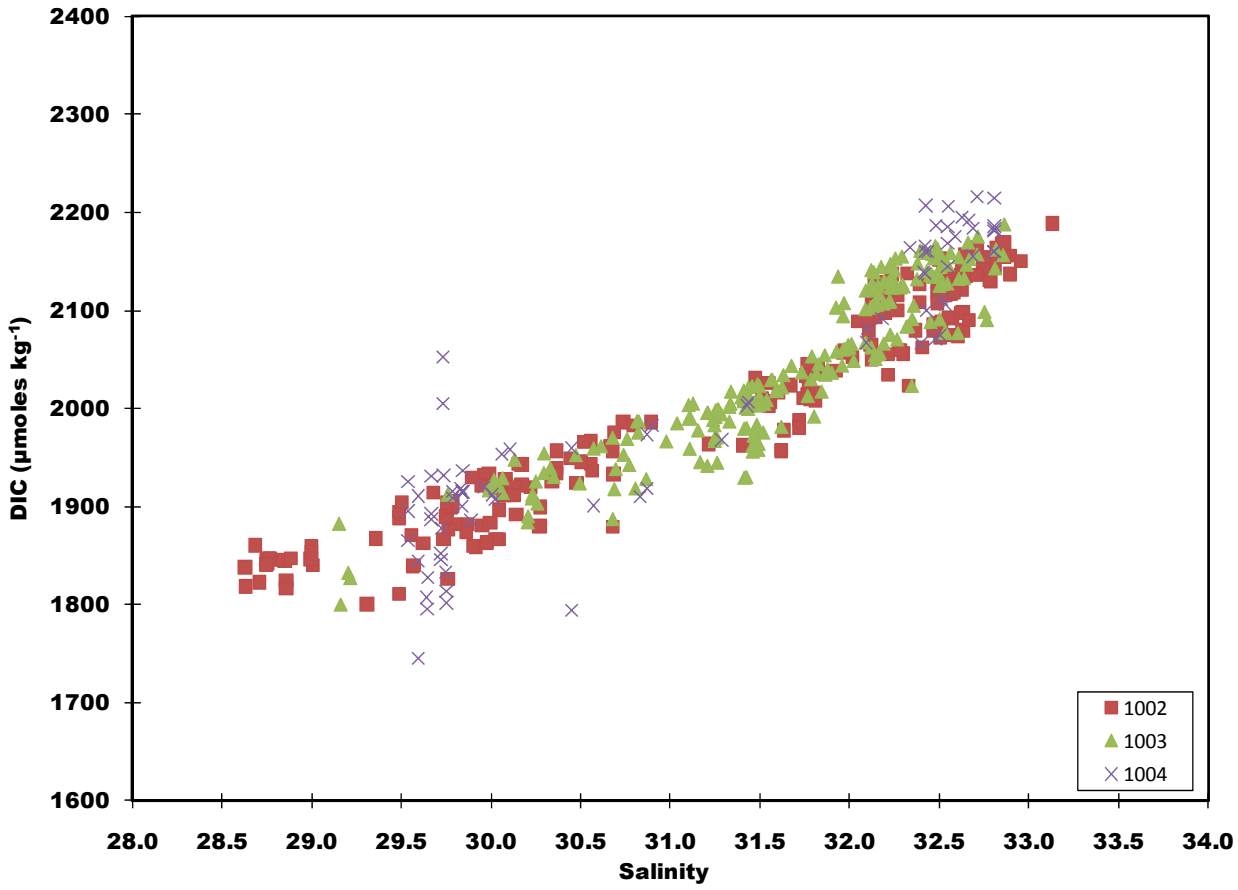

Figure 3 – Observed DIC (µmoles kg-1) vs. salinity in August (1002), September (1003), and October (1004) in the study area.

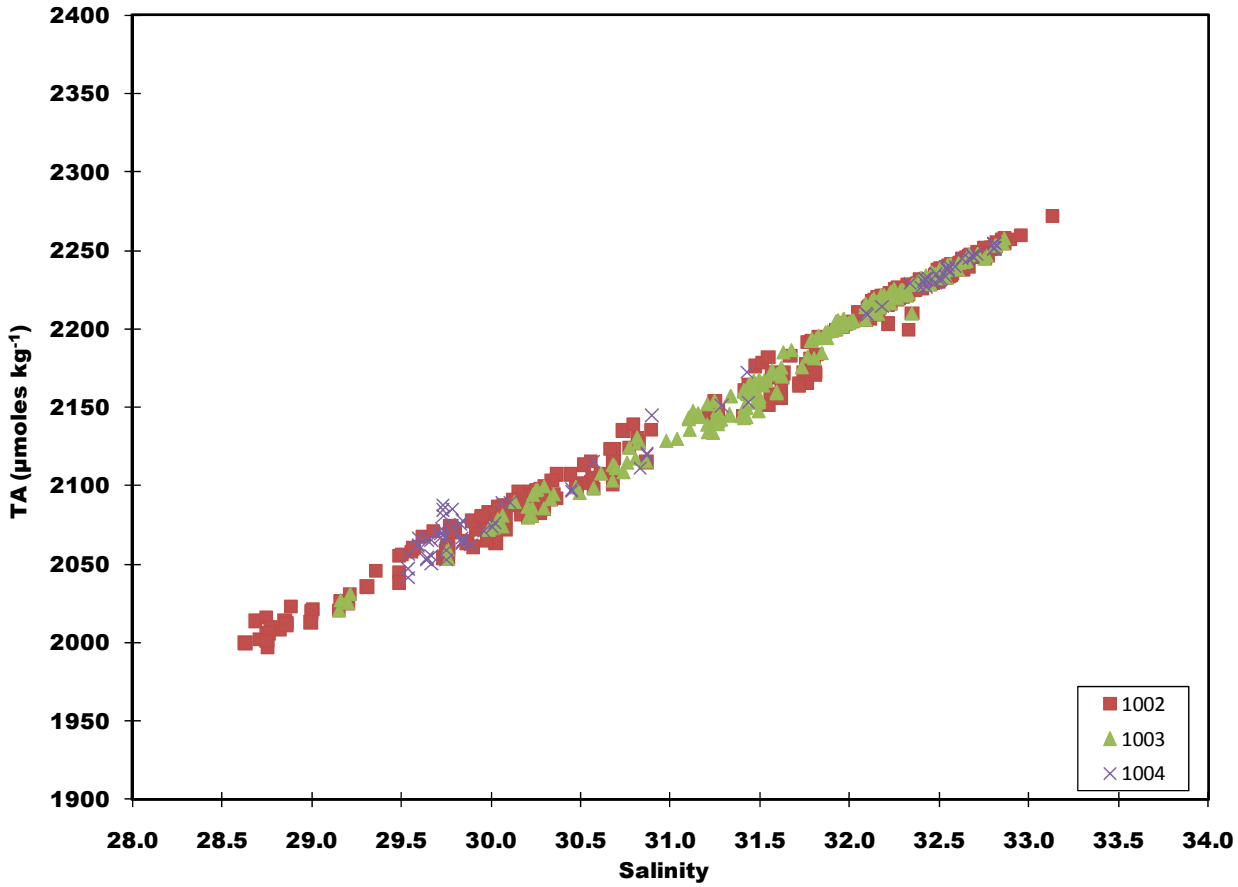

Figure 4 - Observed TA (µmoles kg-1) vs. salinity in August (1002), September (1003), and October (1004) in the study area.

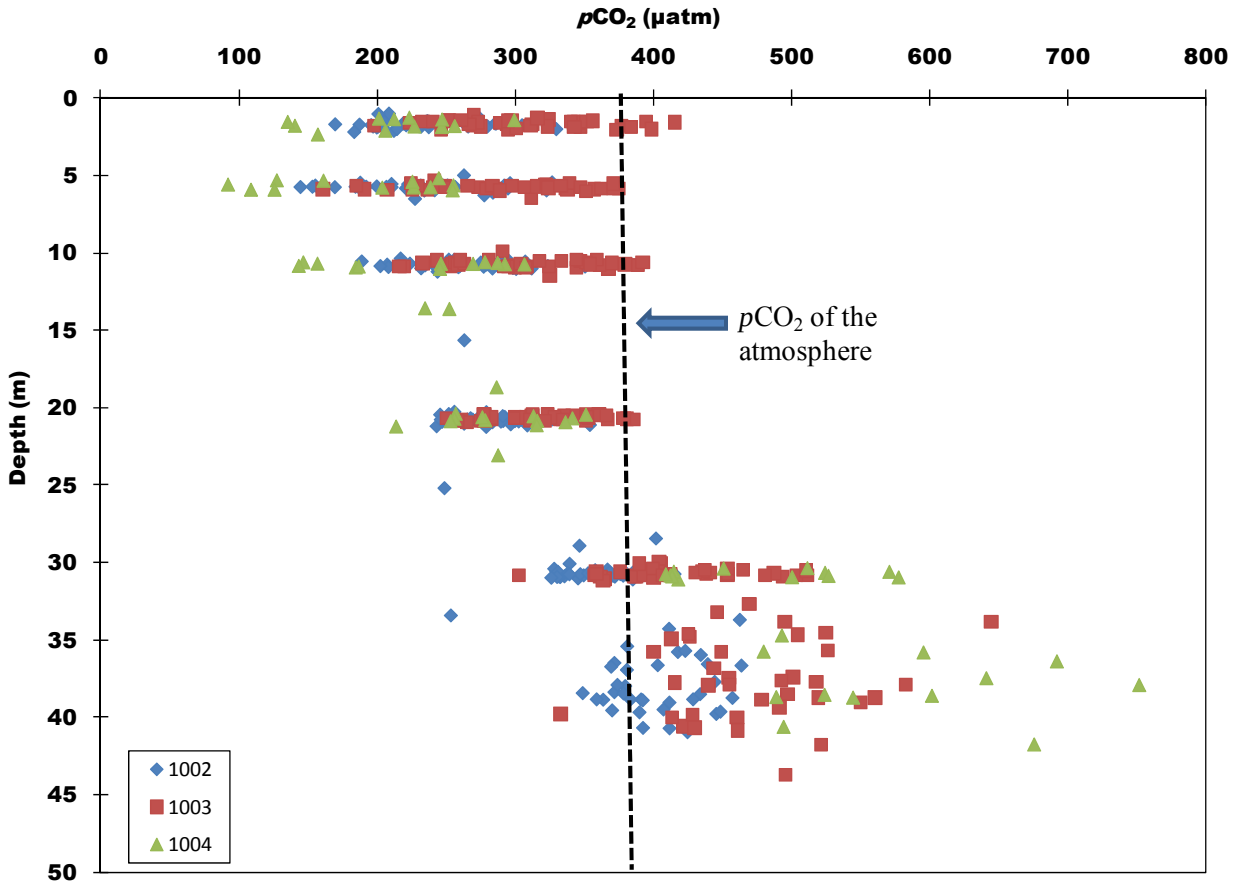

Figure 5 – Calculated pCO_2 (µatm) vs. depth (m) in August (1002), September (1003), and October (1004) in the study area. The black dashed line shows the average concentration of atmospheric CO_2.

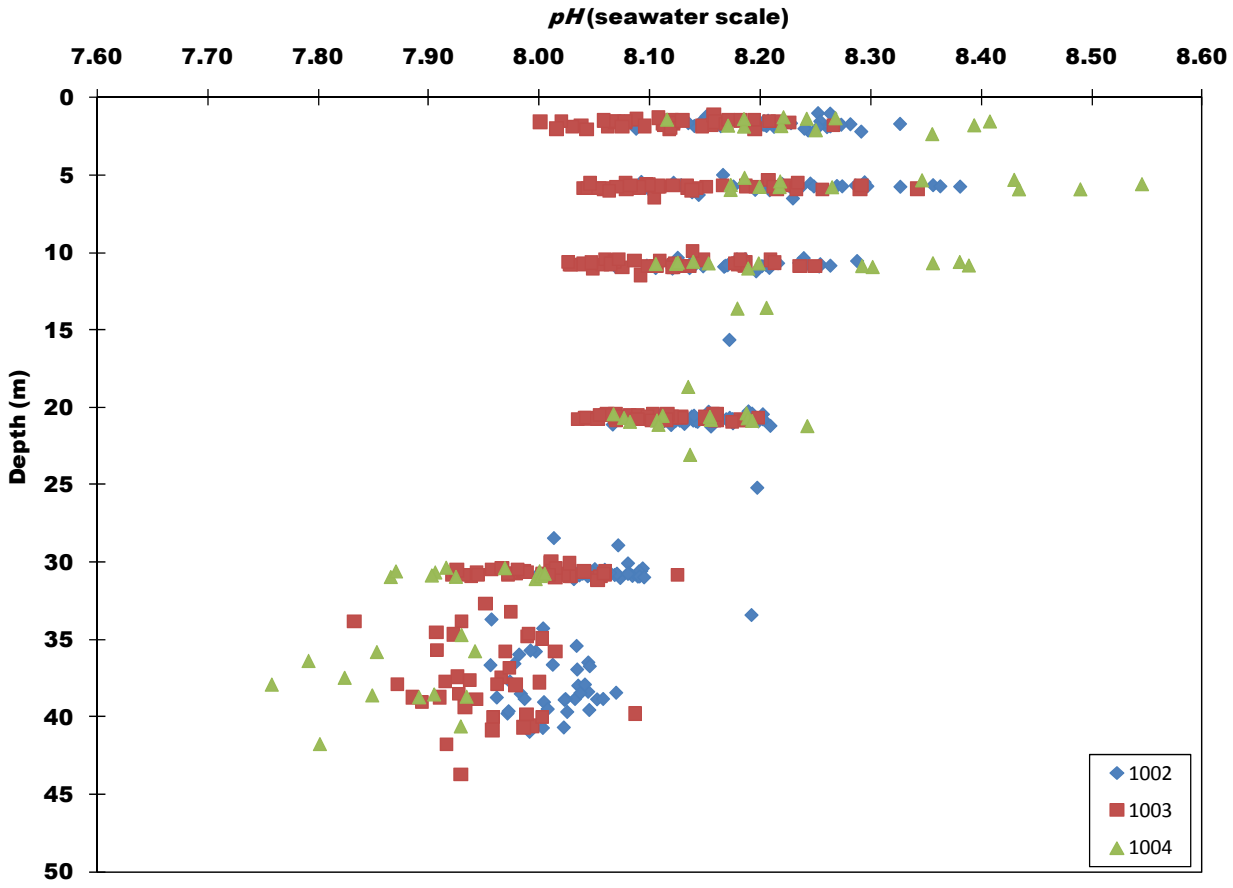

Figure 6 – Calculated *pH* (seawater scale) vs. depth (m) in August (1002), September (1003), and October (1004) in the study area.

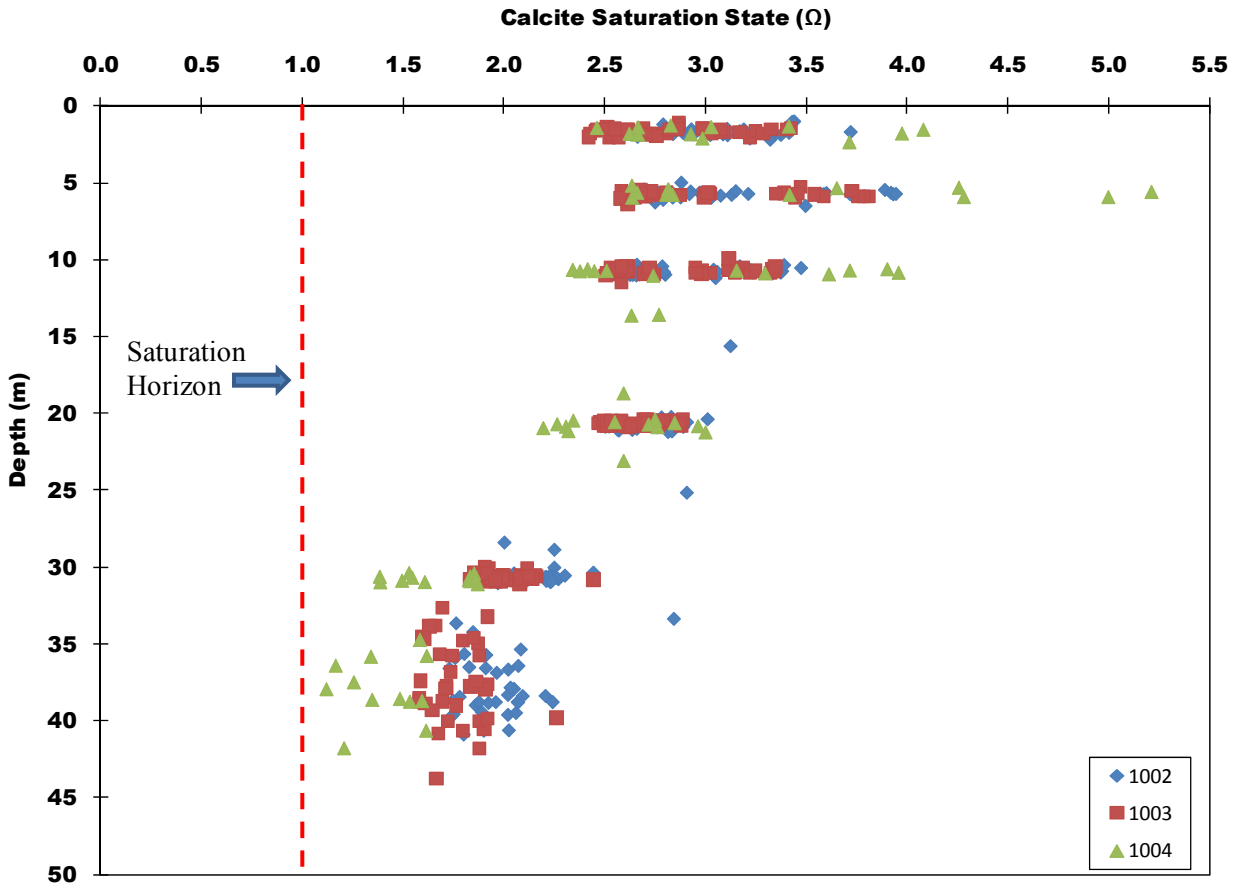

Figure 7 – Calculated calcite saturation state (Ω) vs. depth (m) in August (1002), September (1003), and October (1004) in the study area. The red dashed line show the saturation horizon (Ω = 1) for calcite.

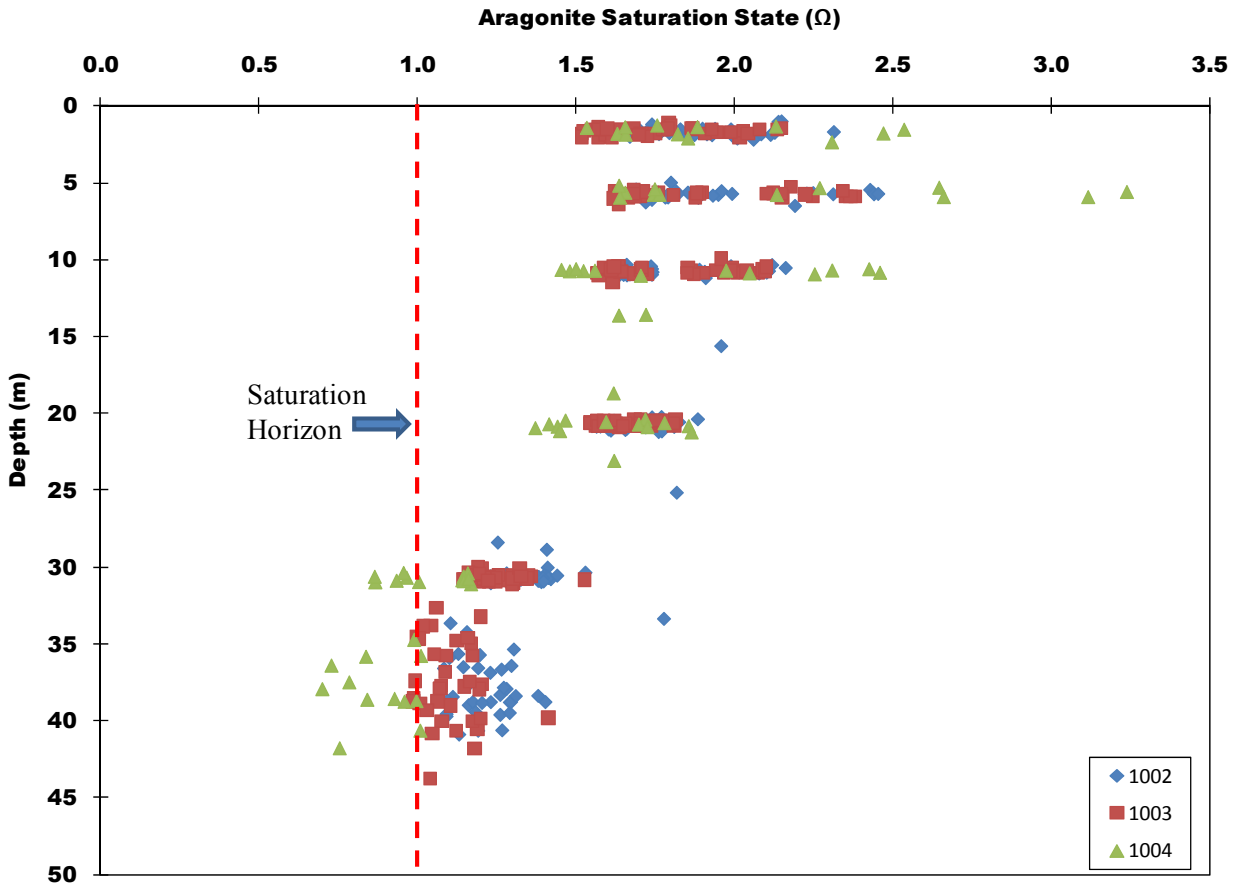

Figure 8 – Calculated aragonite saturation state (Ω) vs. depth (m) in August (1002), September (1003), and October (1004) in the study area. The red dashed line show the saturation horizon (Ω = 1) for aragonite.

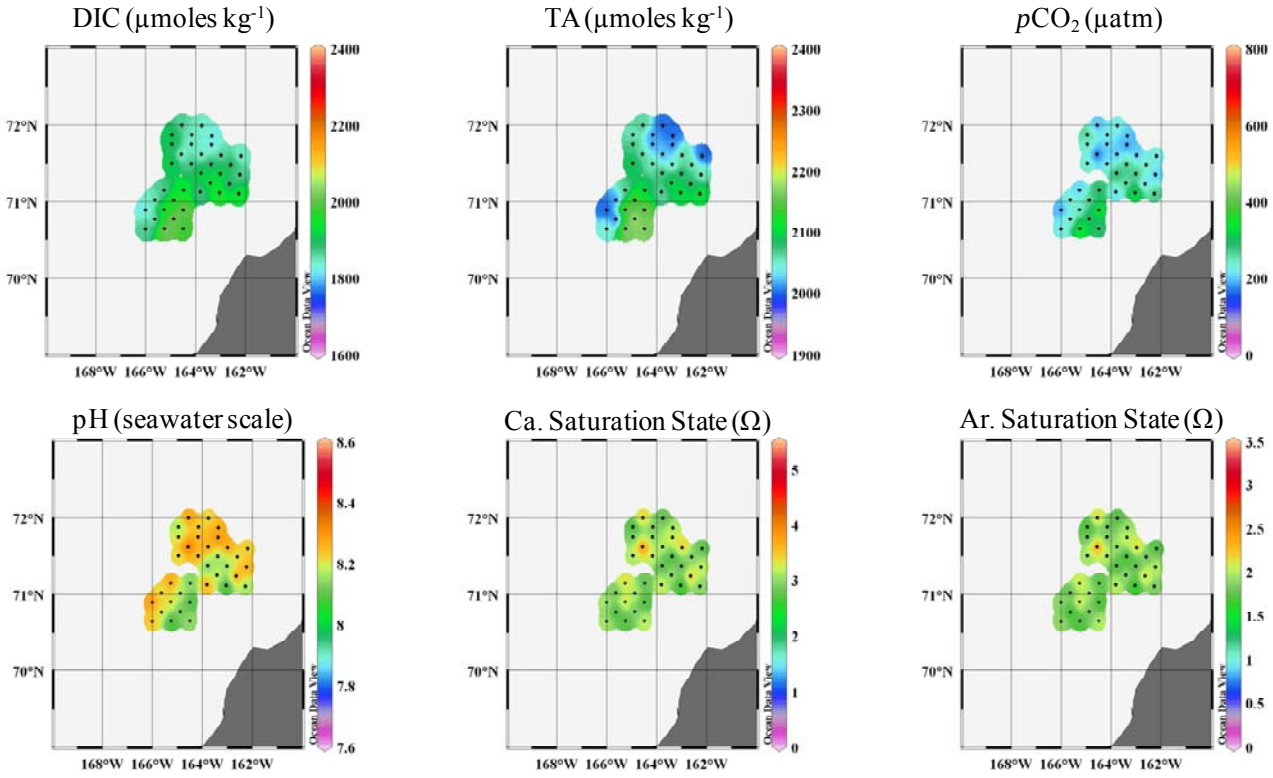

Figure 9 – Observations of DIC and TA (µmoles kg^{-1}) and calculated values for pCO_2 (µatm), *p*H (seawater scale), calcite saturation state (Ω), and aragonite saturation state (Ω) at the surface in August (1002).

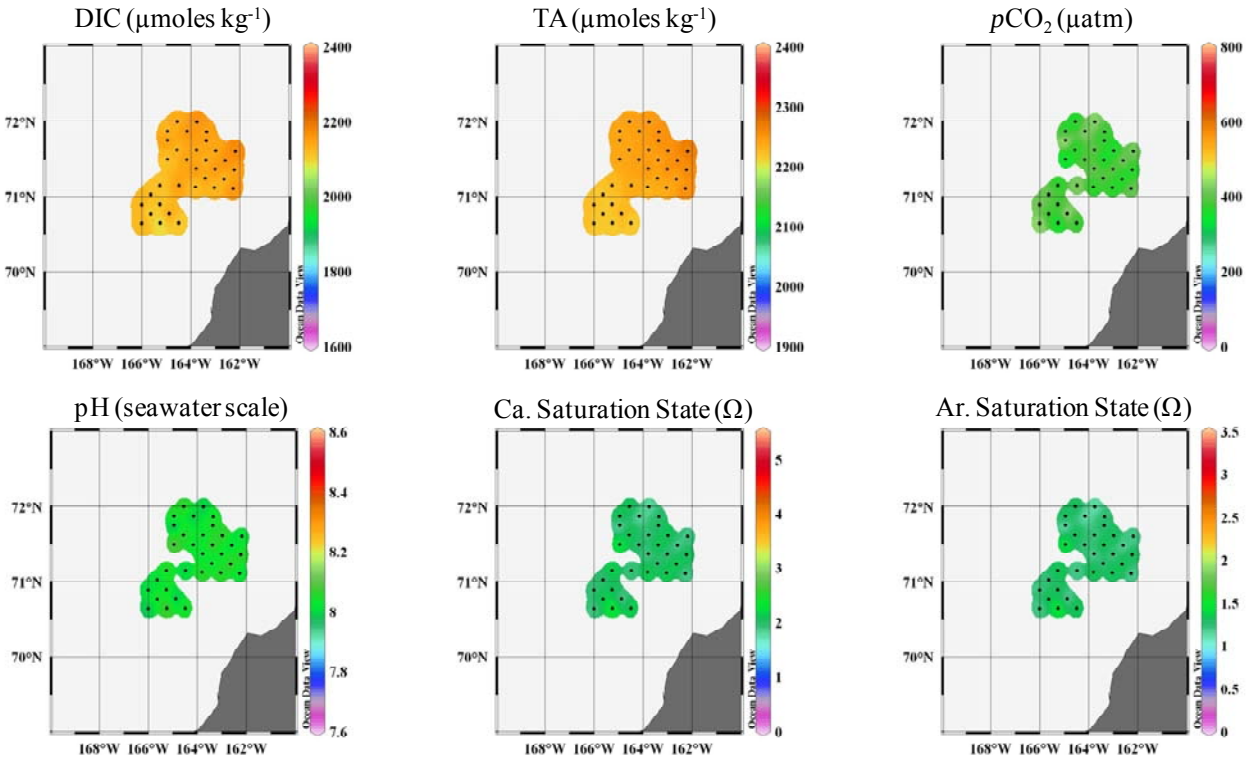

Figure 10 – Observations of DIC and TA (µmoles kg^{-1}) and calculated values for pCO_2 (µatm), *p*H (seawater scale), calcite saturation state (Ω), and aragonite saturation state (Ω) along the bottom in August (1002).

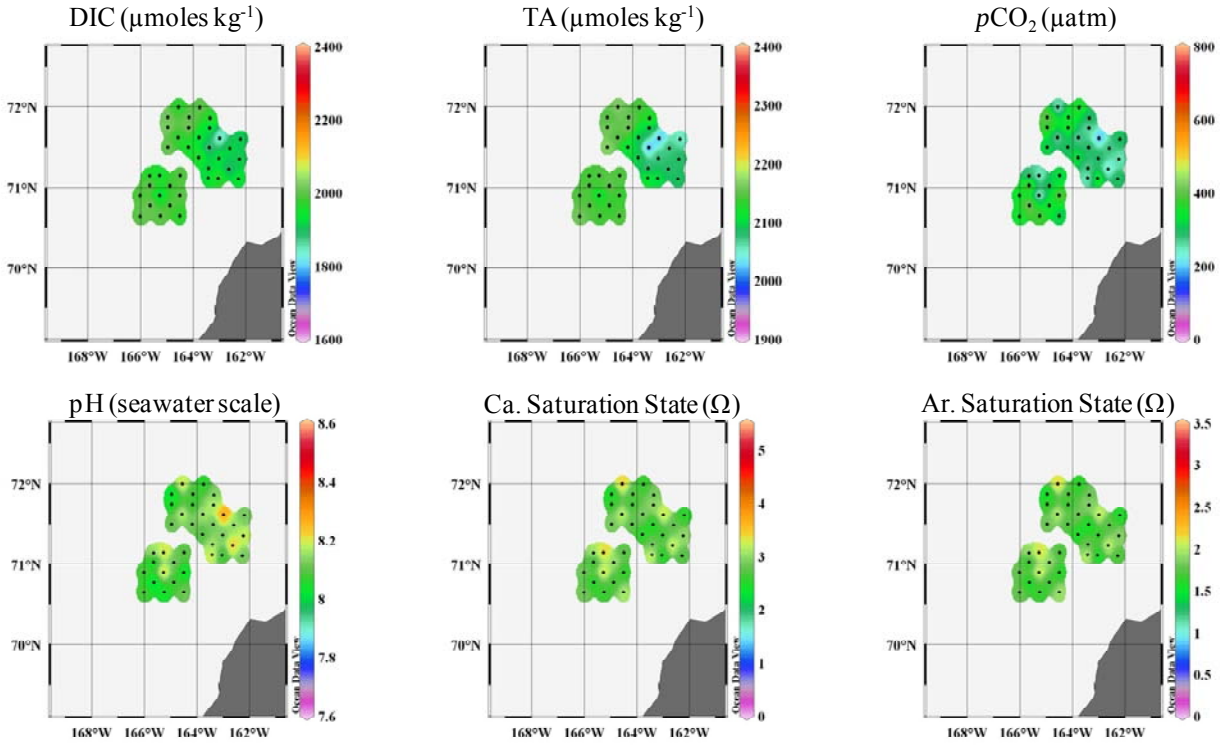

Figure 11 – Observations of DIC and TA (µmoles kg^{-1}) and calculated values for pCO_2 (µatm), *p*H (seawater scale), calcite saturation state (Ω), and aragonite saturation state (Ω) at the surface in September (1003).

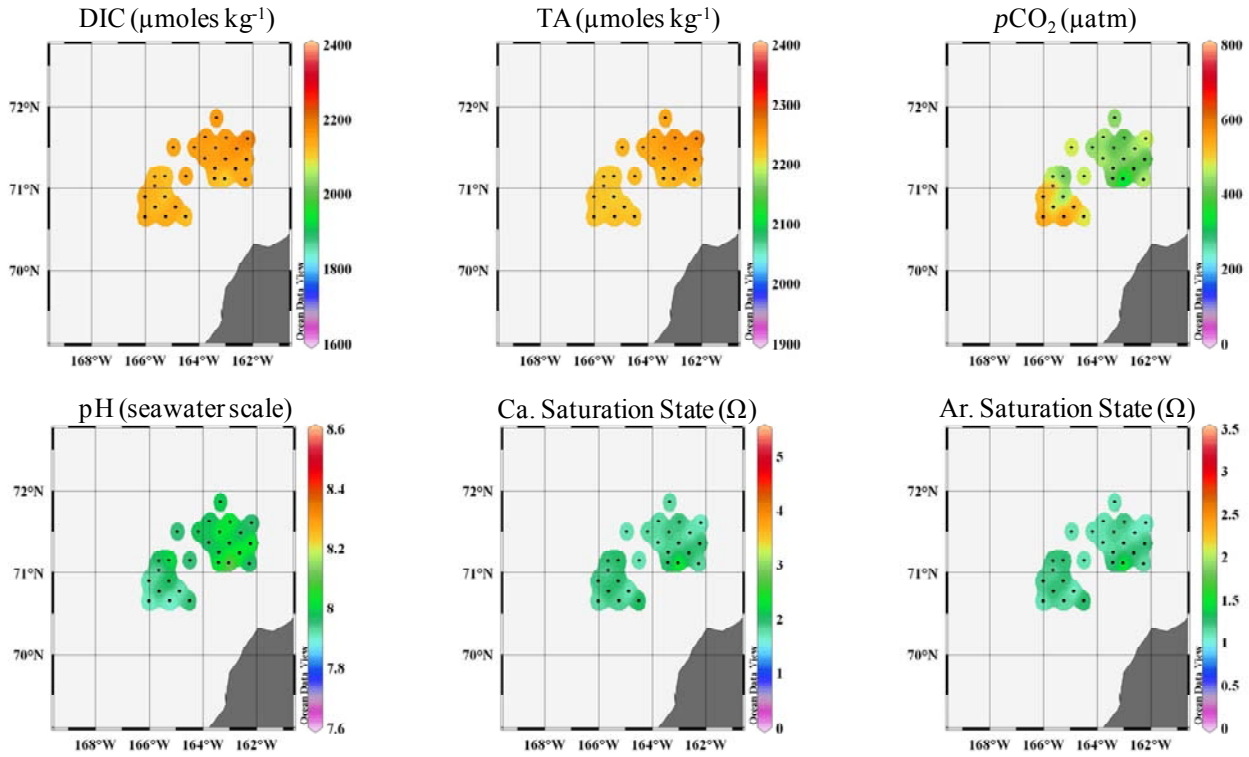

Figure 12 – Observations of DIC and TA (µmoles kg^{-1}) and calculated values for pCO_2 (µatm), *p*H (seawater scale), calcite saturation state (Ω), and aragonite saturation state (Ω) along the bottom in September (1003).

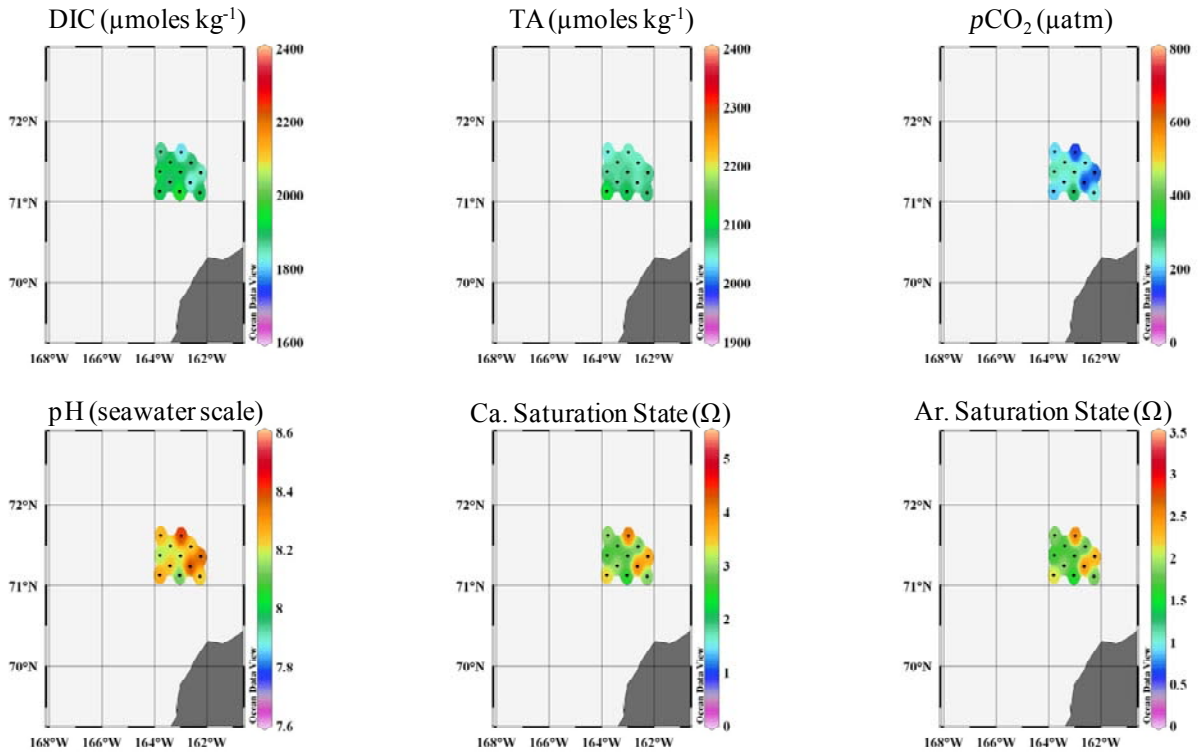

Figure 13 – Observations of DIC and TA (µmoles kg^{-1}) and calculated values for pCO_2 (µatm), *p*H (seawater scale), calcite saturation state (Ω), and aragonite saturation state (Ω) at the surface in October (1004).

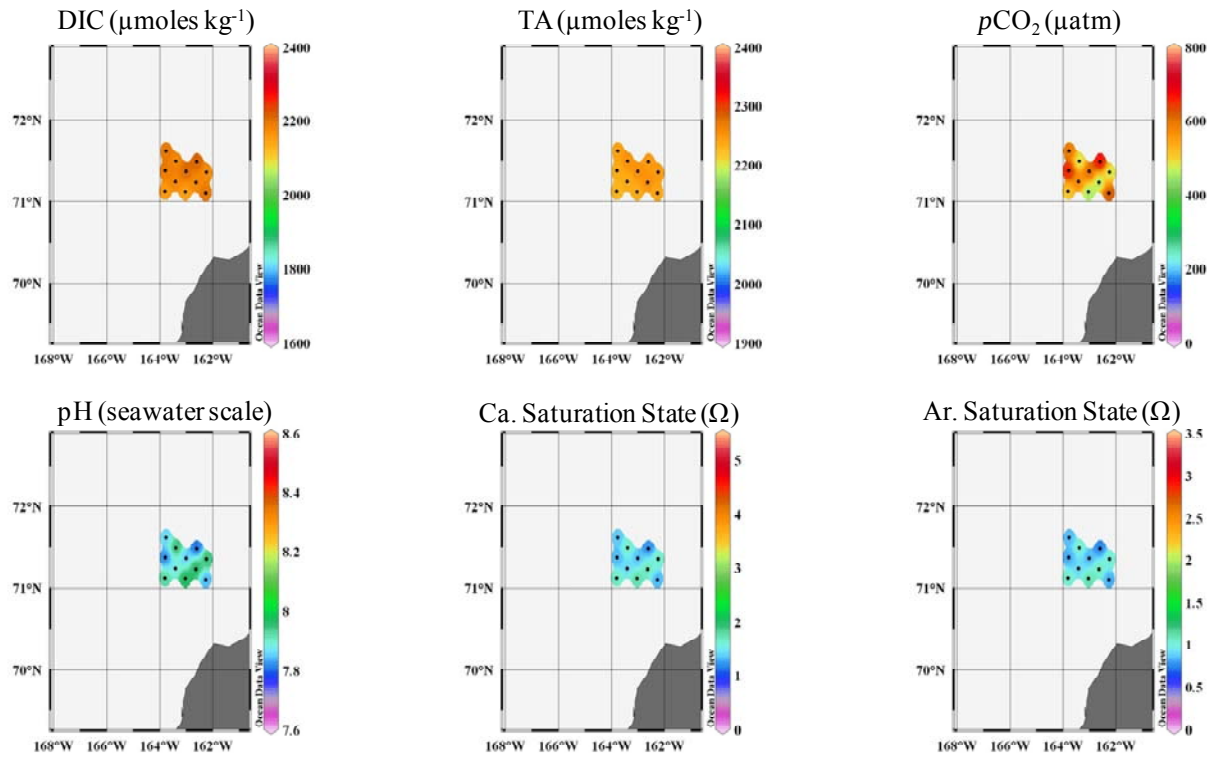

Figure 14 – Observations of DIC and TA (µmoles kg^{-1}) and calculated values for pCO_2 (µatm), *p*H (seawater scale), calcite saturation state (Ω), and aragonite saturation state (Ω) along the bottom in October (1004).

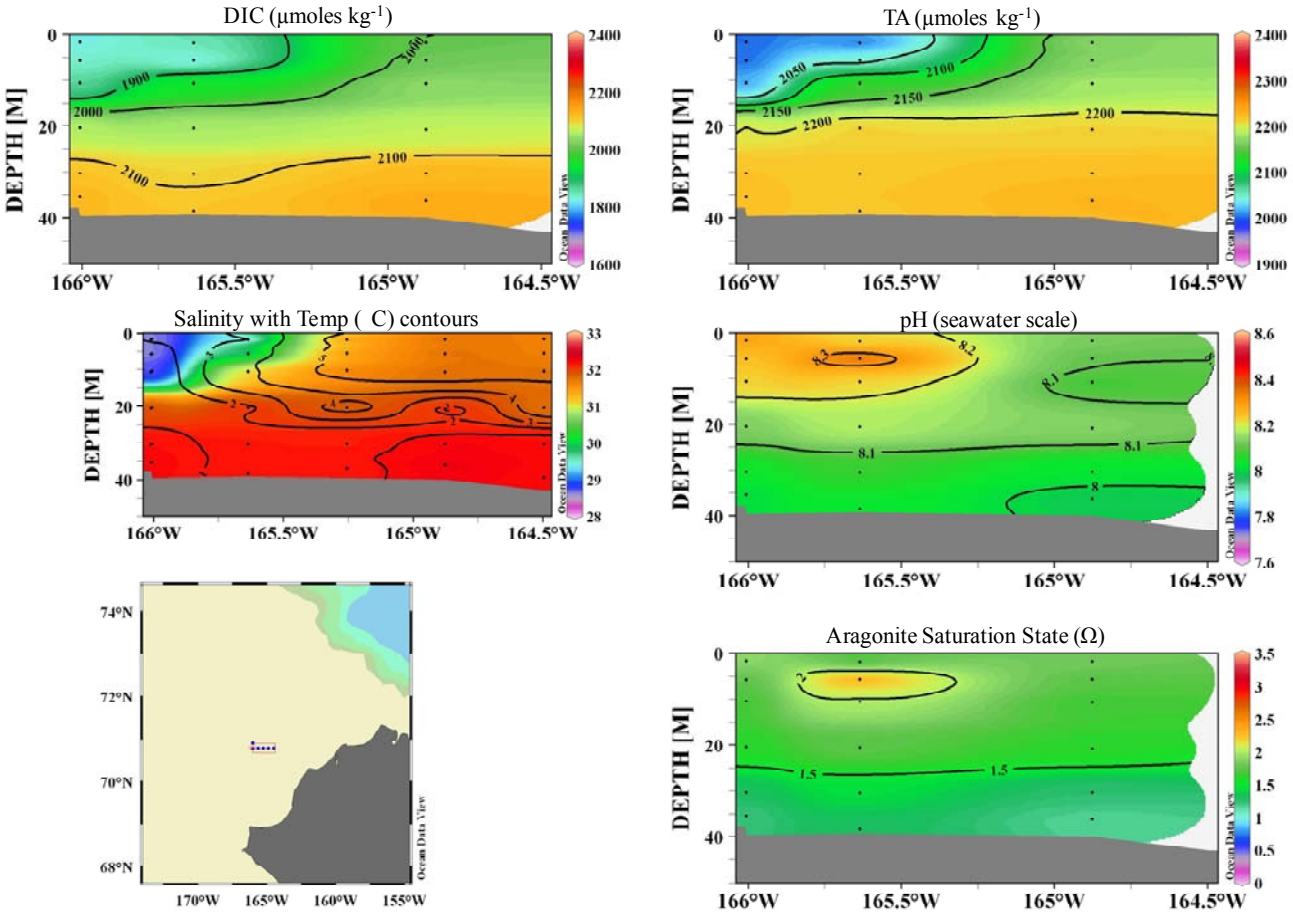

Figure 15 – Observations of DIC and TA (µmoles kg^{-1}) along with salinity and temperature (°C) with calculated values for *p*H (seawater scale) and aragonite saturation state (Ω) in a representative east-west section in the Klondike area in August (1002).

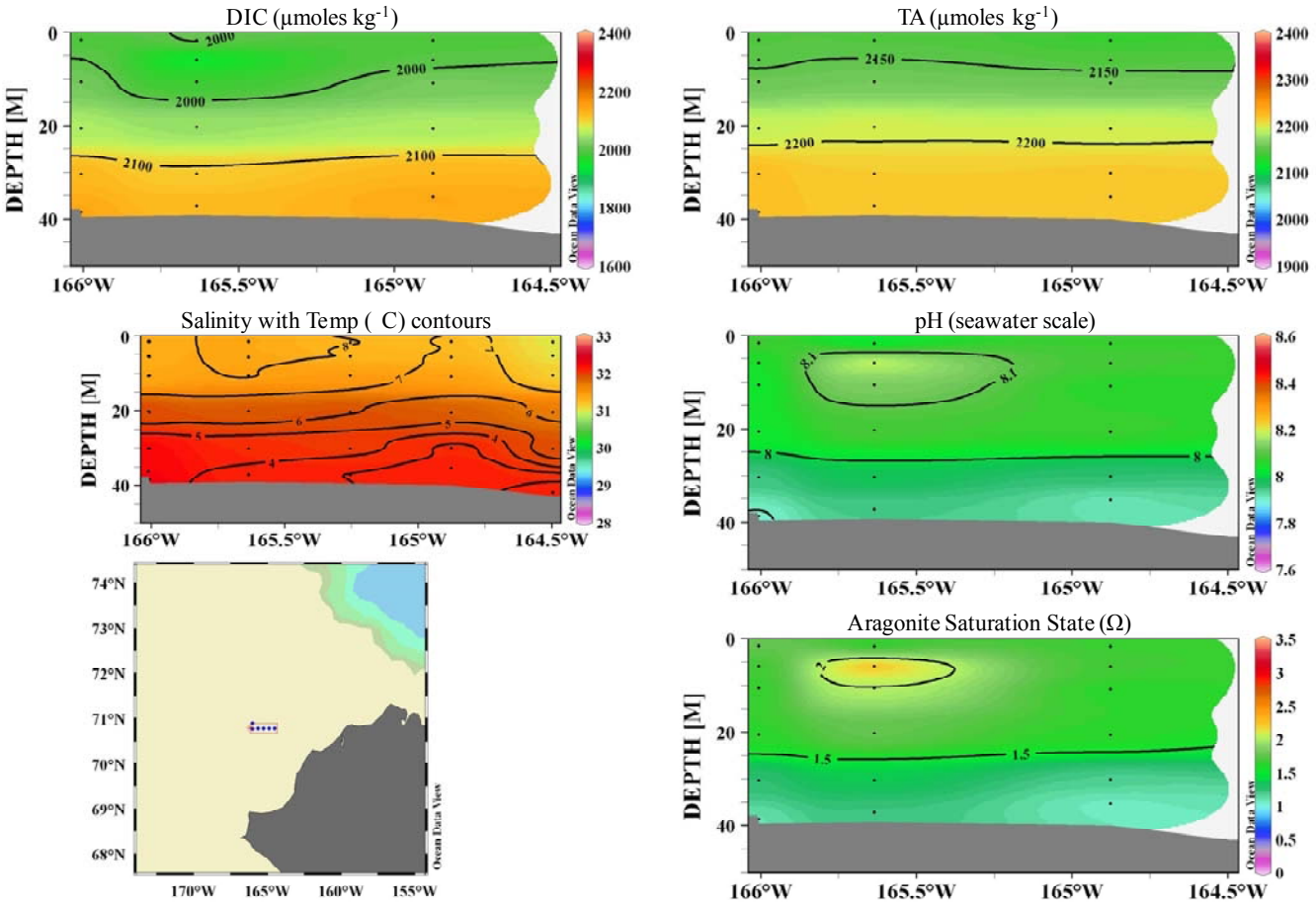

Figure 16 – Observations of DIC and TA (µmoles kg^{-1}) along with salinity and temperature (°C) with calculated values for *p*H (seawater scale) and aragonite saturation state (Ω) in a representative east-west section in the Klondike area in September (1003).

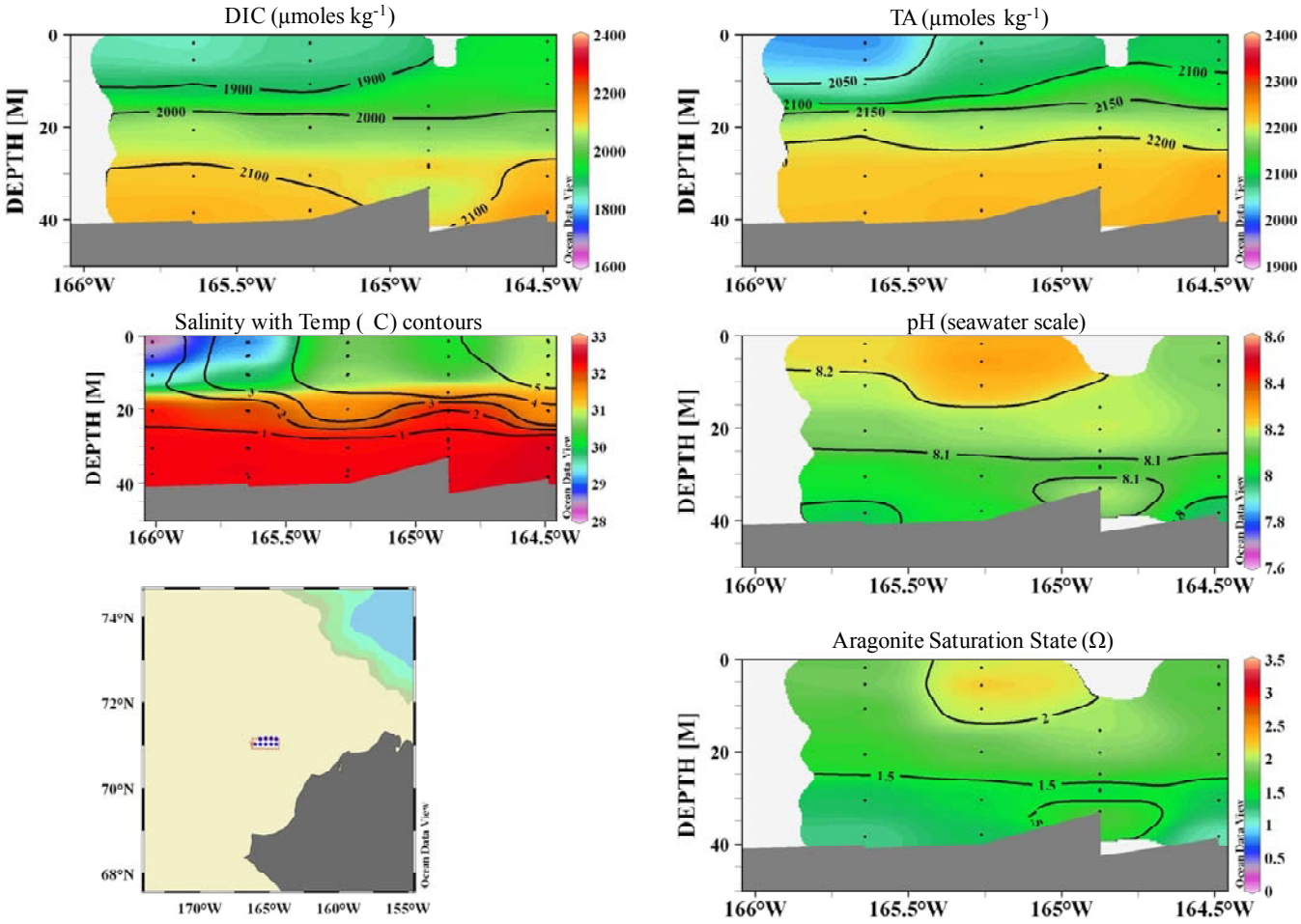

Figure 17 – Observations of DIC and TA (µmoles kg^{-1}) along with salinity and temperature (°C) with calculated values for *p*H (seawater scale) and aragonite saturation state (Ω) in a representative east-west section in the Burger area in August (1002).

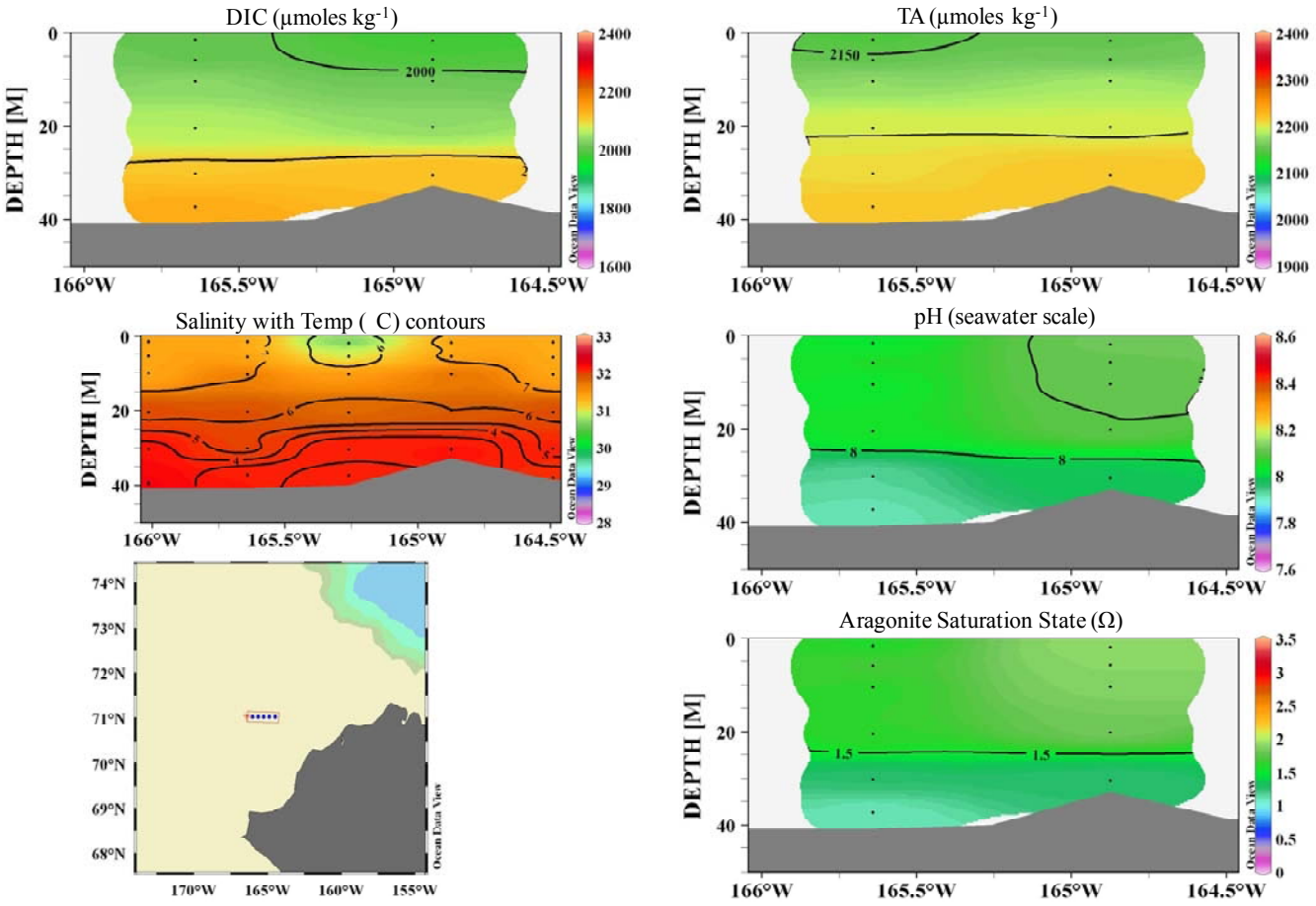

Figure 18 – Observations of DIC and TA (µmoles kg^{-1}) along with salinity and temperature (°C) with calculated values for *p*H (seawater scale) and aragonite saturation state (Ω) in a representative east-west section in the Burger area in September (1003).

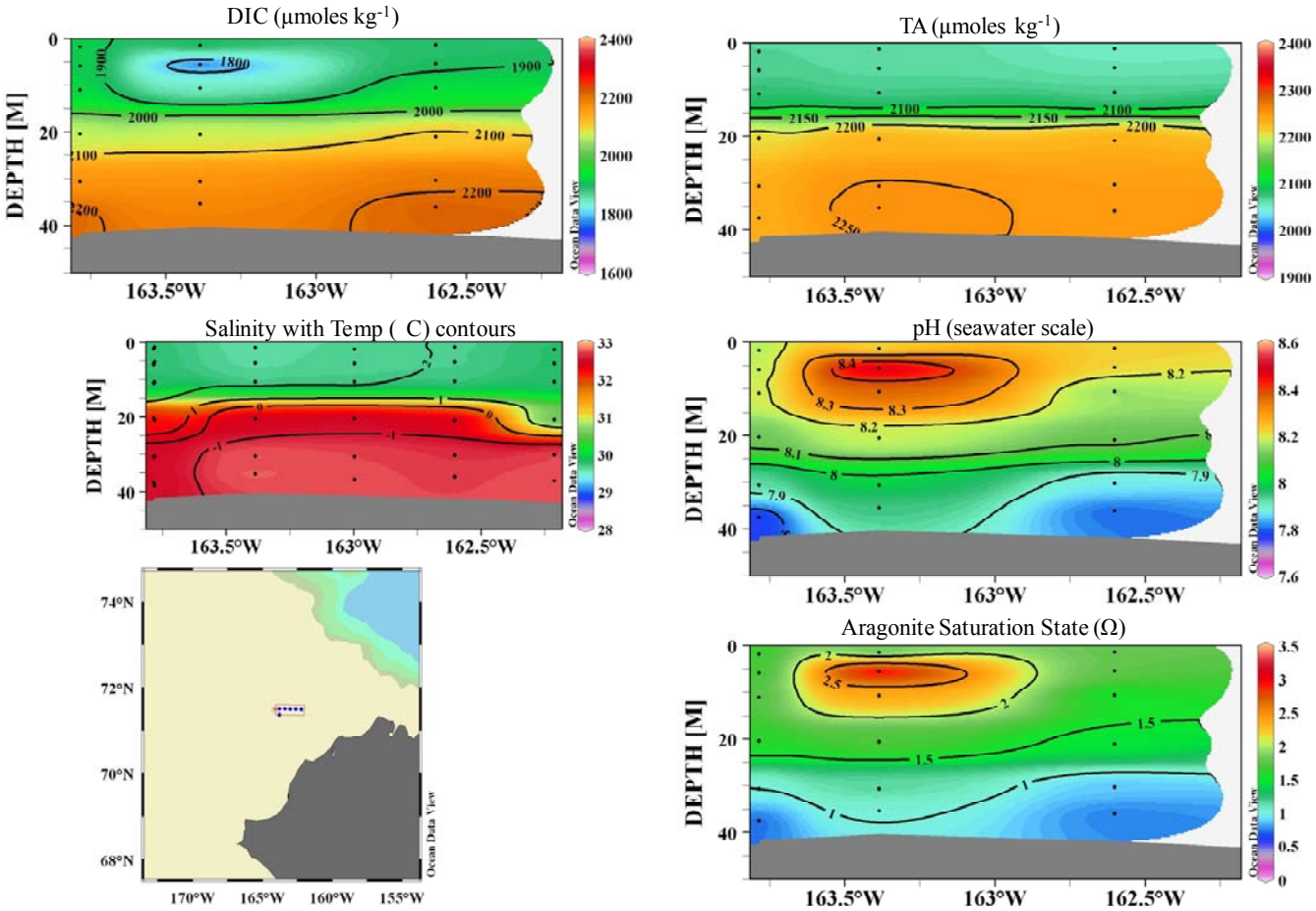

Figure 19 – Observations of DIC and TA (µmoles kg^{-1}) along with salinity and temperature (°C) with calculated values for *p*H (seawater scale) and aragonite saturation state (Ω) in a representative east-west section in the Burger area in October (1004).

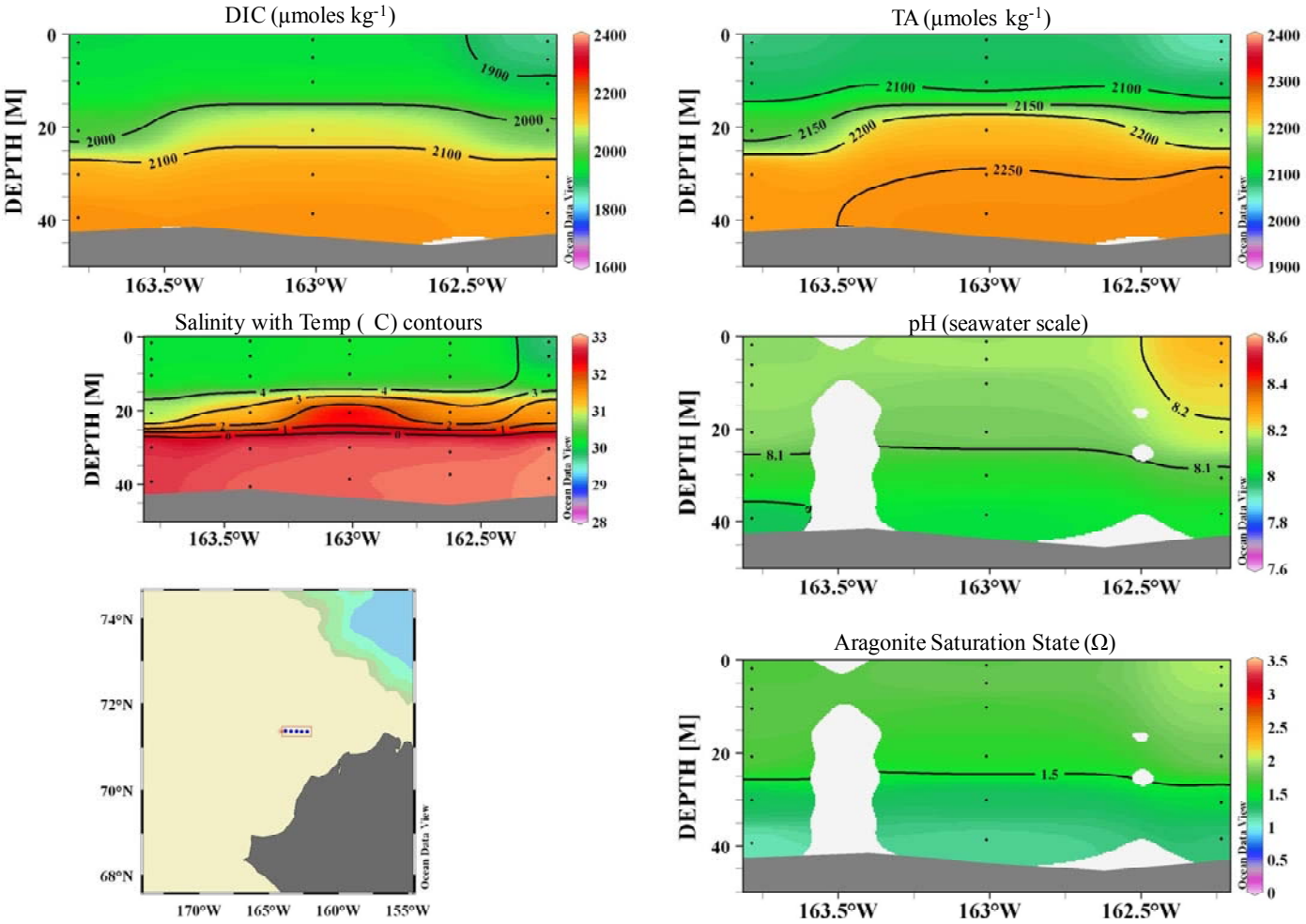

Figure 20 – Observations of DIC and TA (µmoles kg^{-1}) along with salinity and temperature (°C) with calculated values for *p*H (seawater scale) and aragonite saturation state (Ω) in a representative east-west section in the Statoil area in August (1002).

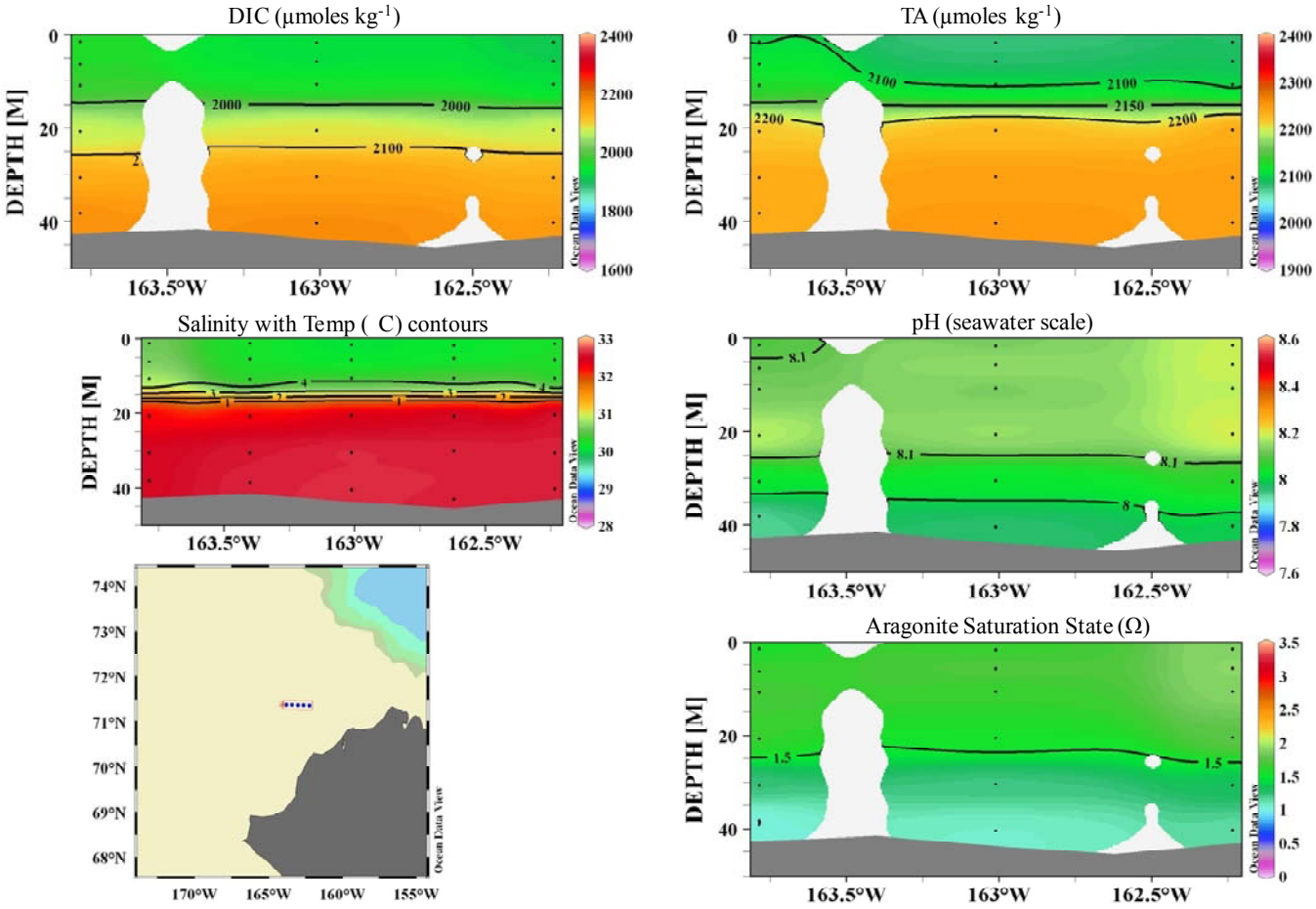

Figure 21 – Observations of DIC and TA (µmoles kg^{-1}) along with salinity and temperature (°C) with calculated values for *p*H (seawater scale) and aragonite saturation state (Ω) in a representative east-west section in the Statoil area in September (1003).

Table 1 – Observed vales for DIC and TA (µmoles kg^{-1}) and calculated values for pH (seawater scale), pCO_2 (µatm) and calcite/aragonite saturation states (Ω) at the surface and near the bottom in the Berger area for August, September and October.

August - 1002								September - 1003						October - 1004					
STNNBR	Depth	DIC µmol kg^{-1}	TA µmol kg^{-1}	pH sw scale	pCO2 µatm	Ca. Sat. Ω	Ar. Sat. Ω	DIC µmol kg^{-1}	TA µmol kg^{-1}	pH sw scale	pCO2 µatm	ΩCa Ω	ΩAr Ω	DIC µmol kg^{-1}	TA µmol kg^{-1}	pH sw scale	pCO2 µatm	ΩCa Ω	ΩAr Ω
BF003	Bottom	2128	2235	8.04	380	2.05	1.28	2104	2228	8.09	333	2.26	1.41	2160	2232	7.93	495	1.61	1.01
BF003	Surface	1957	2101	8.09	326	2.59	1.62	1970	2103	8.06	347	2.43	1.52	1960	2097	8.12	299	2.46	1.53
BF005	Bottom	2169	2257	7.99	425	1.80	1.13	2147	2223	7.93	496	1.66	1.04	2206	2241	7.80	676	1.21	0.75
BF005	Surface	1936	2105	8.17	266	2.94	1.84	1934	2085	8.12	297	2.69	1.68	1907	2076	8.22	227	2.93	1.82
BF007	Bottom	2142	2237	8.00	412	1.90	1.19	2148	2229	7.96	461	1.72	1.08	2186	2235	7.85	602	1.35	0.84
BF007	Surface	1924	2099	8.18	256	3.03	1.90	1914	2074	8.16	269	2.80	1.75	1886	2062	8.24	212	3.03	1.88
BF009	Bottom	2133	2241	8.05	370	2.06	1.29	2146	2241	8.00	413	1.88	1.17	2183	2254	7.93	489	1.59	1.00
BF009	Surface	1880	2083	8.25	209	3.44	2.15	1890	2080	8.23	224	3.25	2.03	1814	2053	8.39	141	3.97	2.47
BF011	Bottom	2165	2247	7.97	445	1.74	1.09	2165	2235	7.93	497	1.58	0.99	2207	2232	7.76	752	1.12	0.70
BF011	Surface	1918	2072	8.14	280	2.72	1.70	1959	2098	8.09	324	2.51	1.57	1915	2064	8.17	256	2.62	1.63
BF013	Bottom	2164	2255	8.01	412	1.86	1.16	2169	2247	7.96	461	1.67	1.05	2215	2255	7.82	641	1.25	0.78
BF013	Surface	1923	2082	8.15	273	2.79	1.74	1927	2073	8.12	294	2.61	1.63	1915	2067	8.19	247	2.66	1.66
BF015	Bottom	2156	2257	8.03	383	1.96	1.23	2154	2242	7.99	430	1.80	1.12	2184	2246	7.91	524	1.48	0.93
BF015	Surface	1867	2054	8.26	205	3.19	1.99	1908	2081	8.18	252	2.99	1.87	1846	2067	8.36	157	3.71	2.31
BF017	Bottom	2136	2245	8.05	364	2.07	1.29	2152	2247	8.01	400	1.88	1.17	2181	2255	7.94	480	1.62	1.01
BF017	Surface	1888	2038	8.16	266	2.65	1.65	1882	2020	8.12	289	2.45	1.53	1911	2062	8.19	247	2.66	1.65
BF019	Bottom	2169	2255	7.98	434	1.78	1.11	2175	2248	7.94	478	1.61	1.01	2216	2247	7.79	693	1.16	0.73
BF019	Surface	1890	2059	8.20	236	2.93	1.83	1916	2072	8.15	275	2.74	1.71	1887	2050	8.22	223	2.83	1.76
BF021	Bottom	2148	2245	8.01	403	1.91	1.19	2155	2238	7.97	449	1.74	1.09	2195	2245	7.85	596	1.34	0.84
BF021	Surface	1840	2021	8.26	200	3.11	1.93	1930	2094	8.16	270	2.87	1.79	1865	2041	8.25	206	2.98	1.85
BF023	Bottom	2146	2252	8.05	372	2.02	1.26	2162	2253	8.00	416	1.83	1.15	2168	2238	7.93	493	1.58	0.99
BF023	Surface	1859	2061	8.26	201	3.43	2.14	1832	2025	8.27	198	3.28	2.04	1807	2053	8.41	135	4.08	2.54
BF025	Bottom	2189	2272	7.97	448	1.75	1.09	2187	2258	7.93	501	1.59	0.99	2052	2088				
BF025	Surface	1841	2001	8.22	219	2.78	1.72	1912	2053	8.12	295	2.52	1.57	2006	2153	8.14	288	2.59	1.62

Table 2 - Observed vales for DIC and TA (µmoles kg^{-1}) and calculated values for pH (seawater scale), pCO_2 (µatm) and calcite/aragonite saturation states (Ω) at the surface and near the bottom in the Klondike area for August and September.

August - 1002								September - 1003					
STNNBR	Depth	DIC µmol kg^{-1}	TA µmol kg^{-1}	pH sw scale	pCO2 µatm	Ca. Sat. Ω	Ar. Sat. Ω	DIC µmol kg^{-1}	TA µmol kg^{-1}	pH sw scale	pCO2 µatm	ΩCa Ω	ΩAr Ω
KF001	Bottom	2129	2220	7.97	444	1.86	1.16	2144	2221	7.89	561	1.70	1.06
KF001	Surface	1867	2046	8.23	221	3.07	1.91	1999	2158	8.08	342	2.83	1.78
KF003	Bottom	2094	2215	8.06	359	2.24	1.40	2144	2222	7.87	583	1.71	1.07
KF003	Surface	2014	2166	8.08	341	2.71	1.70	1998	2140	8.04	377	2.59	1.63
KF005	Bottom	2118	2223	8.02	392	2.02	1.27	2130	2221	7.92	521	1.88	1.18
KF005	Surface	1981	2163	8.15	286	3.17	1.99	1967	2143	8.11	312	3.09	1.95
KF007	Bottom	2108	2217	8.02	391	2.07	1.29	2120	2215	7.94	493	1.91	1.20
KF007	Surface	1847	1997	8.20	232	2.63	1.63	2011	2144	8.00	416	2.46	1.55
KF009	Bottom	2138	2228	7.98	439	1.83	1.14	2141	2217	7.91	526	1.68	1.05
KF009	Surface	2008	2172	8.12	305	2.89	1.81	1988	2134	8.07	346	2.61	1.64
KF011	Bottom	2123	2219	8.00	418	1.91	1.20	2140	2223	7.89	550	1.76	1.11
KF011	Surface	1818	1999	8.28	188	3.09	1.91	1986	2144	8.08	341	2.82	1.77
KF013	Bottom	2108	2218	8.03	381	2.08	1.30	2120	2216	7.98	440	1.91	1.19
KF013	Surface	1958	2156	8.21	238	3.37	2.12	1918	2113	8.22	233	3.32	2.08
KF015	Bottom	2137	2221	7.96	462	1.76	1.10	2134	2205	7.83	645	1.66	1.04
KF015	Surface	2002	2151	8.09	330	2.66	1.67	1995	2134	8.03	384	2.54	1.59
KF017	Bottom	2125	2219	7.99	429	1.88	1.17	2139	2218	7.91	518	1.72	1.07
KF017	Surface	1845	2009	8.21	231	2.84	1.76	2007	2143	8.02	395	2.50	1.57
KF019	Bottom	2117	2220	8.01	402	2.00	1.25	2126	2216	7.94	481	1.84	1.15
KF019	Surface	1963	2144	8.17	263	3.12	1.96	1980	2153	8.11	311	3.03	1.91
KF023	Bottom	2116	2226	8.04	378	2.09	1.31	2123	2219	7.99	429	1.92	1.20
KF023	Surface	1867	2064	8.26	201	3.35	2.09	1945	2144	8.21	240	3.41	2.14
KF025	Bottom	2153	2236	7.96	457	1.75	1.09	2155	2225	7.91	520	1.58	0.99
KF025	Surface	1934	2092	8.14	286	2.79	1.74	1989	2142	8.10	324	2.72	1.71

Table 3 - Observed vales for DIC and TA (µmoles kg^{-1}) and calculated values for pH (seawater scale), pCO_2 (µatm) and calcite/aragonite saturation states (Ω) at the surface and near the bottom in the Statoil area for August and September.

August - 1002								September - 1003					
STNNBR	Depth	DIC µmol kg^{-1}	TA µmol kg^{-1}	pH sw scale	pCO2 µatm	Ca. Sat. Ω	Ar. Sat. Ω	DIC µmol kg^{-1}	TA µmol kg^{-1}	pH sw scale	pCO2 µatm	ΩCa Ω	ΩAr Ω
SF001	Bottom	2118	2237	8.07	349	2.21	1.38	2158	2234	7.93	491	1.64	1.03
SF001	Surface	1911	2091	8.21	237	3.11	1.94	2005	2167	8.11	316	2.87	1.80
SF003	Bottom	2148	2243	8.01	407	1.89	1.18	2153	2234	7.96	455	1.71	1.07
SF003	Surface	1871	2058	8.24	215	3.21	2.00	1952	2108	8.12	300	2.76	1.72
SF005	Bottom	2133	2241	8.04	374	2.03	1.27	2144	2238	8.00	413	1.87	1.17
SF005	Surface	1840	2061	8.33	170	3.72	2.32	1964	2147	8.17	267	3.17	1.99
SF007	Bottom	2153	2236	7.96	464	1.73	1.08	2153	2223	7.91	525	1.59	1.00
SF007	Surface	1901	2071	8.20	237	2.92	1.82	2018	2159	8.04	374	2.57	1.61
SF009	Bottom	2154	2246	8.00	411	1.85	1.15	2157	2236	7.95	470	1.69	1.06
SF009	Surface	1841	2016	8.25	204	3.02	1.87	2012	2157	8.07	352	2.61	1.64
SF011	Bottom	2150	2251	8.04	381	1.96	1.23	2149	2237	7.99	426	1.80	1.12
SF011	Surface	1816	2011	8.29	184	3.32	2.06	1923	2095	8.17	261	2.98	1.87
SF013	Bottom	2130	2240	8.05	372	2.07	1.30	2128	2224	7.97	446	1.92	1.20
SF013	Surface	1904	2055	8.16	263	2.66	1.65	2013	2144	8.02	399	2.42	1.52
SF015	Bottom	2157	2243	7.99	423	1.80	1.13	2162	2236	7.93	495	1.63	1.02
SF015	Surface	1846	2013	8.22	221	2.89	1.79	2003	2153	8.08	343	2.70	1.70
SF017	Bottom	2155	2251	8.02	392	1.92	1.20	2158	2241	7.97	444	1.74	1.09
SF017	Surface	1823	2002	8.26	197	3.09	1.91	1966	2128	8.13	295	2.86	1.79
SF019	Bottom	2136	2242	8.05	369	2.02	1.26	2140	2232	7.99	426	1.85	1.16
SF019	Surface	1864	2065	8.27	196	3.41	2.13	1962	2161	8.19	251	3.42	2.15
SF021	Bottom	2164	2249	7.98	434	1.76	1.10	2161	2232	7.92	504	1.61	1.00
SF021	Surface	1841	2001	8.21	224	2.79	1.73	1999	2139	8.06	356	2.55	1.60

Table 4 – The differences (August minus September and September minus October values) in observed DIC and TA (µmoles kg^{-1}) and calculated values for pH (seawater scale), pCO_2 (µatm) and calcite/aragonite saturation states (Ω) at the surface and near the bottom in the Burger area. Positive Δ values indicate an increase in concentration or carbonate parameter from August to September and September to October. Negative values indicate an increase in concentration or carbonate parameter.

Differences Between August and September (1002 - 1003)								Differences Between September and October (1002 - 1003)					
STNNBR	Depth	ΔDIC µmol kg^{-1}	ΔTA µmol kg^{-1}	ΔpH sw scale	ΔpCO2 µatm	ΔΩCa Ω	ΔΩAr Ω	ΔDIC µmol kg^{-1}	ΔTA µmol kg^{-1}	ΔpH sw scale	ΔpCO2 µatm	ΔΩCa Ω	ΔΩAr Ω
BF003	Bottom	23	7	-0.05	47	-0.21	-0.13	-55	-4	0.16	-162	0.65	0.41
BF003	Surface	-13	-2	0.03	-22	0.16	0.10	10	7	-0.05	48	-0.03	-0.02
BF005	Bottom	22	34	0.06	-72	0.14	0.09	-59	-17	0.13	-180	0.46	0.29
BF005	Surface	2	19	0.04	-31	0.25	0.16	27	9	-0.10	70	-0.24	-0.14
BF007	Bottom	-6	8	0.05	-49	0.18	0.11	-39	-5	0.11	-141	0.38	0.23
BF007	Surface	11	25	0.02	-13	0.23	0.15	28	12	-0.09	57	-0.22	-0.13
BF009	Bottom	-13	1	0.04	-43	0.18	0.12	-37	-14	0.07	-76	0.29	0.18
BF009	Surface	-9	3	0.03	-15	0.19	0.12	76	27	-0.17	83	-0.73	-0.44
BF011	Bottom	-1	13	0.05	-52	0.16	0.10	-42	3	0.17	-255	0.46	0.29
BF011	Surface	-41	-27	0.05	-44	0.21	0.13	44	35	-0.08	68	-0.11	-0.06
BF013	Bottom	-5	8	0.05	-50	0.19	0.11	-46	-8	0.13	-180	0.42	0.26
BF013	Surface	-4	8	0.03	-21	0.18	0.11	12	7	-0.06	47	-0.06	-0.03
BF015	Bottom	2	15	0.05	-47	0.16	0.11	-30	-4	0.08	-94	0.31	0.20
BF015	Surface	-41	-27	0.07	-46	0.20	0.12	62	14	-0.17	95	-0.72	-0.44
BF017	Bottom	-16	-2	0.04	-37	0.19	0.12	-29	-7	0.07	-80	0.26	0.16
BF017	Surface	6	18	0.03	-23	0.20	0.12	-28	-42	-0.06	42	-0.21	-0.13
BF019	Bottom	-6	8	0.04	-45	0.17	0.10	-41	0	0.15	-214	0.45	0.28
BF019	Surface	-27	-13	0.06	-39	0.19	0.12	29	21	-0.07	52	-0.09	-0.05
BF021	Bottom	-7	7	0.04	-46	0.17	0.10	-40	-7	0.12	-147	0.40	0.25
BF021	Surface	-90	-73	0.10	-70	0.24	0.14	65	53	-0.09	64	-0.11	-0.06
BF023	Bottom	-16	-2	0.04	-44	0.19	0.11	-6	15	0.07	-78	0.25	0.16
BF023	Surface	27	36	0.00	3	0.15	0.10	25	-28	-0.14	62	-0.80	-0.49
BF025	Bottom	1	14	0.05	-53	0.16	0.10	135	170				
BF025	Surface	-71	-52	0.11	-76	0.26	0.15	-94	-100	-0.02	7	-0.07	-0.05

Table 5 – The differences (August minus September values) in observed DIC and TA (µmoles kg^{-1}) and calculated values for pH (seawater scale), pCO_2 (µatm) and calcite/aragonite saturation states (Ω) at the surface and near the bottom in the Klondike area. Positive Δ values indicate an increase in concentration or carbonate parameter from August to September. Negative values indicate an increase in concentration or carbonate parameter.

Differences Between August and September (1002 - 1003)							
STNNBR	Depth	ΔDIC µmol kg^{-1}	ΔTA µmol kg^{-1}	ΔpH sw scale	ΔpCO2 µatm	ΔΩCa Ω	ΔΩAr Ω
KF001	Bottom	-15	-1	0.09	-116	0.16	0.10
KF001	Surface	-132	-113	0.15	-122	0.25	0.14
KF003	Bottom	-51	-6	0.19	-224	0.53	0.33
KF003	Surface	16	26	0.04	-36	0.11	0.07
KF005	Bottom	-12	2	0.11	-129	0.14	0.09
KF005	Surface	14	20	0.03	-27	0.08	0.05
KF007	Bottom	-12	2	0.09	-102	0.15	0.09
KF007	Surface	-165	-147	0.20	-184	0.17	0.08
KF009	Bottom	-3	11	0.07	-87	0.15	0.09
KF009	Surface	20	39	0.05	-41	0.28	0.18
KF011	Bottom	-18	-3	0.10	-133	0.15	0.09
KF011	Surface	-168	-145	0.20	-153	0.27	0.14
KF013	Bottom	-12	2	0.06	-59	0.17	0.11
KF013	Surface	40	43	0.00	5	0.05	0.04
KF015	Bottom	3	16	0.12	-182	0.11	0.06
KF015	Surface	7	17	0.06	-54	0.13	0.08
KF017	Bottom	-14	0	0.07	-89	0.16	0.10
KF017	Surface	-162	-134	0.19	-164	0.34	0.19
KF019	Bottom	-9	5	0.07	-79	0.16	0.10
KF019	Surface	-18	-8	0.06	-48	0.09	0.05
KF023	Bottom	-7	7	0.05	-50	0.18	0.11
KF023	Surface	-78	-80	0.06	-39	-0.06	-0.05
KF025	Bottom	-2	11	0.05	-63	0.17	0.11
KF025	Surface	-55	-50	0.04	-37	0.06	0.03

Table 6 – The differences (August minus September values) in observed DIC and TA (µmoles kg^{-1}) and calculated values for pH (seawater scale), pCO_2 (µatm) and calcite/aragonite saturation states (Ω) at the surface and near the bottom in the Statoil area. Positive Δ values indicate an increase in concentration or carbonate parameter from August to September. Negative values indicate an increase in concentration or carbonate parameter.

Differences Between August and September (1002 - 1003)							
STNNBR	Depth	ΔDIC	ΔTA	ΔpH	ΔpCO2	ΔΩCa	ΔΩAr
		µmol kg^{-1}	µmol kg^{-1}	sw scale	µatm	Ω	Ω
SF001	Bottom	-40	3	0.14	-143	0.56	0.35
SF001	Surface	-93	-76	0.10	-79	0.24	0.14
SF003	Bottom	-5	9	0.05	-48	0.18	0.11
SF003	Surface	-81	-50	0.12	-86	0.45	0.27
SF005	Bottom	-11	3	0.04	-39	0.16	0.10
SF005	Surface	-124	-87	0.16	-97	0.55	0.33
SF007	Bottom	0	13	0.05	-61	0.13	0.08
SF007	Surface	-117	-88	0.16	-137	0.36	0.21
SF009	Bottom	-3	10	0.05	-58	0.15	0.10
SF009	Surface	-171	-140	0.19	-147	0.41	0.23
SF011	Bottom	1	14	0.05	-45	0.17	0.10
SF011	Surface	-107	-84	0.12	-77	0.34	0.20
SF013	Bottom	3	16	0.07	-74	0.15	0.10
SF013	Surface	-109	-89	0.14	-135	0.24	0.14
SF015	Bottom	-6	8	0.06	-72	0.17	0.11
SF015	Surface	-157	-141	0.15	-122	0.19	0.10
SF017	Bottom	-3	10	0.05	-52	0.19	0.12
SF017	Surface	-143	-126	0.13	-97	0.23	0.12
SF019	Bottom	-3	10	0.06	-56	0.17	0.11
SF019	Surface	-98	-96	0.08	-56	-0.01	-0.02
SF021	Bottom	4	17	0.06	-70	0.15	0.10
SF021	Surface	-158	-138	0.16	-132	0.24	0.13

References

Among, R.M.W., 2004. The role of dissolved organic matter for the organic carbon cycle in the Arctic Ocean, in *The Organic Carbon Cycle in the Arctic Ocean*, edited by R.S. Stein and R.W. Macdonald, pp. 83–99, Springer, New York.

Anderson, L.G., and Kaltin, S., 2001. Carbon fluxes in the Arctic Ocean - potential impact by climate change. *Polar Research*, **20**(2), 225-232.

Andersson, A.J., and Mackenzie, F.T., 2004. Shallow-water oceans : a source or sink for atmospheric CO_2? *Frontiers in Ecology and the Environment*, **2**(7), 348–353.

Andreev, A.G., Chen, C.-T.A., and Sereda, N.A., 2010. The distribution of the carbonate parameters in the waters of Anadyr Bay of the Bering Sea and in the western part of the Chukchi Sea. *Oceanology*, **50**(1), 39-50.

Azetsu-Scott, K., Clarke, A., Falkner, K., Hamilton, J., Jones, E.P., Lee, C., Petrie, B., Prinsenberg, S., Starr, M., and, Yeats, P. , 2010. Calcium carbonate saturation states in the waters of the Canadian Arctic Archipelago and the Labrador Sea. *Journal of Geophysical Research-Oceans*, **115**, C11021, doi:10.1029/2009JC005917.

Bates, N.R., 2001. Interannual variability of oceanic CO_2 and biogeochemical properties in the Western North Atlantic subtropical gyre. *Deep-Sea Research II*, **48**, 1507–1528.

Bates, N.R., Best, M.H.P., and Hansell, D.A., 2005a. Spatio-temporal distribution of dissolved inorganic carbon and net community production in the Chukchi and Beaufort Seas. *Deep-Sea Research II,* **52**(22-24), 3303-3323, doi:10.1016/j.dsr2.2005.10.005.

Bates, N.R., Best, M.H.P., and Hansell, D.A., 2006b. Suspended Particulate Organic Matter (sPOM) data from Shelf-Basin Interactions (SBI) survey cruises in the Chukchi and Beaufort Seas during 2004. http://www.eol.ucar.edu/projects/sbi/all_data.shtml.

Bates, N.R., 2006. Air-sea carbon dioxide fluxes and the continental shelf pump of carbon in the Chukchi Sea adjacent to the Arctic Ocean. *Journal of Geophysical Research (Oceans)*, **111**, C10013, doi 10.129/2005JC003083, 12 Oct. 2006.

Bates, N.R., and Mathis, J.T., 2009. The Arctic Ocean marine carbon cycle: Evaluation of air-sea carbon dioxide exchanges, ocean acidification impacts and potential feedbacks. *Biogeosciences*, **6**(11), 2433-2459.

Bates, N.R., 2007. Interannual variability of the oceanic CO_2 sink in the subtropical gyre of the North Atlantic Ocean over the last two decades. *Journal of Geophysical Research (Oceans),* **112** (C9), C09013, doi:2006JC003759, May 4, 2007.

Bates, N.R., Mathis, J.T., and Cooper, L., 2009. The effect of ocean acidification on biologically induced seasonality of carbonate mineral saturation states in the Western Arctic Ocean. *Journal of Geophysical Research (Oceans),* **114**, C11007, doi: 10.1029/2008JC004862.

Bindoff, N.L., Willebrand, J., Artale, V., Cazenave, A., Gregory, J., Gulev, S., Hanawa, K., Le Quéré,C., Levitus, S., Nojiri, Y., Shum, C.K., Talley, L.D., and Unnikrishnan, A., 2007. Observations: Oceanic Climate Change and Sea Level. In: *Climate Change 2007: The Physical Science Basis. Contribution of Working Group I to the Fourth Assessment Report of the Intergovernmental Panel on Climate Change* [Solomon, S., D. Qin, M. Manning, Z. Chen, M. Marquis, K.B. Averyt, M. Tignor and H.L. Miller (eds.)]. Cambridge University Press, Cambridge, United Kingdom and New York, NY, USA.

Buddemeier, R.W., Kleypas, J.A., and Aronson, R.B., 2004. *Coral Reefs and Global Climate*

Change: Potential Contributions of Climate Change to Stresses on Coral Reef Ecosystems, p. 44, (download report at http://www.pewclimate.org/global-warmingindepth/all_reports /coral_reefs/index.cfm). Pew Center on Climate Change.

Byrne, R.H., Mecking, S., Feely, R.A., and Liu, Z., 2010. Direct observations of basin-wide acidification of the North Pacific Ocean. *Geophysical Research Letters*, **37**, L02601, doi:10.1029/2009GL040999.

Cai, W.-J., Chen, L., Chen, B., Gao, Z., Lee, S.H., Chen, J., Pierrot, D., Sullivan, K., Wang, Y., Hu, X., Huang, W.-J., Zhang, Y., Xu, S., Murata, A., Grebmeier, J.M., Jones, E.P., and Zhang, H., 2010. Decrease in the CO_2 uptake capacity in an ice-fee Arctic Ocean basin. *Science*, **329**, 556, doi: 10.1126/science.1189338.

Cai, W-J. 2011. Estuarine and coastal ocean carbon paradox: CO_2 sinks or sites of terrestrial carbon incineration? *Annual Reviews of Marine Science*, **3**, 123-45, doi:10.1146/annurev-marine-120709-142723.

Caldiera, K. and Wickett, M.E., 2003. Anthropogenic carbon and ocean pH. *Nature*, **425**(6956), 365.

Caldiera, K., and Wickett, M.E., 2005. Ocean model predictions of chemistry changes from carbon dioxide emissions to the atmosphere and ocean. *Journal of Geophysical Research – Oceans*, **110**(C9), C09S04, doi:10.1029/2004JC002671.

Carmack, E. and Wassman, P., 2006. Food webs and physical-biological coupling on pan-Arctic shelves: Unifying concepts and comprehensive perspectives. *Progress in Oceanography*, **71**, 446-477. doi:10.1016/j.pocean.2006.10.004.

Chen, L.Q, and Gao, Z.Y, 2007. Spatial variability in the partial pressures of CO_2 in the northern Bering and Chukchi seas. *Deep-Sea Research II*, **54**(23-26), 2619-2629, doi:10.1016/j.dsr2.2007.08.010.

Chierici, M., and Fransson, A., 2009. Calcium carbonate saturation in the surface water of the Arctic Ocean: undersaturation in freshwater influenced shelves. *Biogeosciences*, **6**, 2421-2432.

Coachman, L.K., Aagaard, K., and Tripp, R.B., 1975, *Bering Strait: The Regional Physical Oceanography*, University of Washington Press, Seattle, 169 pp.

Codispoti, L. Flagg, C., and Kelly, V., 2005. Hydrographic conditions during the 2002 SBI process experiments. *Deep-Sea Research II,* **52** (22-24), 3199-3226.

Cooley, S.R., and Doney, S.C., 2009. Anticipating ocean acidification's economic consequences for commercial fisheries. *Environmental Research Letters*, **4**, 024007, doi:10.1088/1748-9326/4/2/024007.

Cooper, L.W., McClelland, J.W., Holmes, R.M., Raymond, P.A., Gibson, J.J., Guay, C.K., and Peterson, B.J., 2008. Flow-weighted values of runoff tracers ($d^{18}O$, DOC, Ba, alkalinity) from the six largest Arctic rivers. *Geophysical Research Letters,* **35**, L18606, doi:10.1029/2008GL035007.

Cota, G.F., Pomeroy, L.R., Harrison, W.G., Jones, E.P., Peters, F., Sheldon W.M., and Weingartner T.R., 1996. Nutrients, primary production and microbial heterotrophy in the southeastern Chukchi Sea: Arctic summer nutrient depletion and heterotrophy. *Marine Ecology Progress Series*, **135** (1-3): 247-258.

Dickson, A.G., and Millero, F.J., 1987. A comparison of the equilibrium constants for the dissociation of carbonic acid in seawater media. *Deep Sea Research Part A*, **34**(10), 1733–1743.

Dickson, A.G., 1990. Standard potential of the reaction AgCl(s) + .5H2(g) = Ag(s) + HCl(aq) and the standard acidity constant of the ion HSO_4^- in synthetic sea water from 273.15 to 318.15 K: *The Journal of Chemical Thermodynamics*, **22**(2), 113-127.

Dickson, A.G., and Goyet, C., Eds., 1994. Handbook of Methods for the Analysis of Various Parameters of the Carbon Dioxide System in Seawater, version 2.0. *Rep. ORNL/CDIAC-74*, U.S. Department Of Energy, Washington, D.C.

Fabry, V.J., Seibel, B.A., Feely, R A., and Orr, J.C., 2008. Impacts of ocean acidification on marine fauna and ecosystem processes. *ICES Journal of Marine Science*, **65**, 414–432.

Fabry, V.J., McClintock, J.B., Mathis, J.T., and Grebmeier, J.M., 2009. Ocean Acidification at high latitudes: the Bellwether. *Oceanography*, **22**(4), 160–171.

Feder, H.M., Jewett S.C., and Blanchard A., 2005. Southeastern Chukchi Sea (Alaska) epibenthos. *Polar Biology*, **28**(5), 402-421.

Feely, R.A., Sabine, C.L., Lee, K., Berelson, W., Keypas, J., Fabry, V J., and Millero, F. J., 2004. Impact of anthropogenic CO_2 on the $CaCO_3$ system in the oceans. *Science*, **305**(5682), 362–266.

Fransson, A., Chierici, M., and Nojiri, Y., 2009. New insights into the spatial variability of the surface water carbon dioxide in varying sea ice conditions in the Arctic Ocean. *Continental Shelf Research*, **29**(10), 1317-1328 doi:10.1016/j.csr.2009.03.008.

Gosselin, M., Levasseur, M., Wheeler, P.A., Horner, R.A., and Booth, B.C., 1997. New measurements of phytoplankton and ice algal production in the Arctic Ocean. *Deep-Sea Research II*, **44**, 1623-1644, doi:10.1016/S0967-0645(97)00054-4.

Grebmeier, J.M., Overland, J.E., Moore, S.E., Farley, E.V., Carmack, E.C., Cooper, L W., Frey, K.E., Helle, J.H., McLaughlin, F.A., and McNutt, S.L., 2006. A major ecosystem shift in the Northern Bering Sea. *Science*, **311**(5766)**,** 1461–1464.

Grebmeier, J.M., Bates, N.R., and Devol, A., 2008. Continental Margins of the Arctic Ocean and Bering Sea. In *North American Continental Margins: A Synthesis and Planning Workshop*. U.S. Carbon Cycle Science Program, Washington D.C., (Editors, B. Hales, W.-J. Cai., B.G. Mitchell, C.L. Sabine and O. Schofield, 120 pp), p. 61-72.

Guo, L., and Macdonald, R.W., 2006. Source and transport of terrigenous organic matter in the upper Yukon River: Evidence from isotope ($\delta^{13}C$, $\Delta^{14}C$, and $\delta^{15}N$) composition of dissolved, colloidal, and particulate phases. *Global Biogeochemical Cycles,* **20**(2), GB2011, doi: 10.1029/2005GB002593.

Hameedi, M.J., 1978. Aspects of water column primary productivity in Chukchi Sea during summer. *Marine Biology*, **48**(10), 37-46.

Hill, V., and Cota, G., 2005. Spatial patterns of primary production on the shelf, slope and basin of the Western Arctic in 2002. *Deep-Sea Research II,* **52**(22-24), 3344-3354, doi:10.1016/j.dsr2.2005.10.001.

Holmes, R.M., McClelland, J.W., Raymond, P.A., Frazer, B.B., Peterson, B.J., and Stieglitz, M., 2008. Lability of DOC transported by Alaskan rivers to the Arctic Ocean. *Geophysical Research Letters,* **35**(3), doi: 10.1029/2007GL032837.

Jutterstrom, S., and Anderson, L.G., 2010. Uptake of CO_2 by the Arctic Ocean in a changing climate. *Marine Chemistry*, **122** (1-4), 96-104.

Lepore, K., Moran, S.B., Grebmeier, J.M., Cooper, L.W., Lalande, C., Maslowski, W., Hill, V.,

Bates, N.R., Hansell, D.A., Mathis, J.T., and Kelly, R.P., 2007. Seasonal and interannual changes in particulate organic carbon export and deposition in the Chukchi Sea. *Journal of Geophysical Research*, **112**, C10024, doi:10.1029/2006JC003555.

Lewis, E.R., and Wallace, D.W.R., 1995. Basic programs for the CO_2 system in seawater. Brookhaven National Laboratory, BNL-61827.

Lobbes, J.M., Fitznar, H.P., and G. Kattner, G., 2000. Biogeochemical characteristics of dissolved and particulate organic matter in Russian rivers entering the Arctic Ocean. *Geochim.Cosmochim.Acta,* **64**(17), 2973-2983.

Løvvorn, J R., Richman, S.E., Grebmeier, J.M., and Cooper, L.W., 2003. Diet and body condition of Spectacled Eiders wintering in pack ice of the Bering Sea. *Polar Biology*, **26**, 259–267.

Mathis, J.T., Pickart, R.S., Hansell, D.A., Kadko, D., Bates, N.R., 2007a. Eddy transport of organic carbon and nutrients from the Chukchi Shelf: Impact on the upper halocline of the western Arctic Ocean. *Journal of Geophysical Research*, **112**, C05011, doi: 10.1029/2006JC003899.

Mathis, J.T., Hansell, D.A., and Bates, N.R., 2009. Interannual variability of dissolved inorganic carbon distribution and net community production during the Western Arctic Shelf-Basin Interactions Project. *Deep-Sea Research II*, **56**(17), 1213-1222, doi:10.1016/j.dsr2.2008.10.017.

Macdonald, R.W. Anderson, L.G., Christensen, J.P., Miller, L.A., Semiletov, I.P., and Stein, R., 2010. Polar Margins: The Arctic Ocean. In *Carbon and Nutrient Fluxes in Continental Margins: A Global Synthesis*. Liu, K.K., Atkinson, L., Quinones, R., and Talue-McManus, L., (editors), Springer, New York, 291-303.

McGuire, A.D., Chapin, F.S., Walsh, J.E., and Wirth, C., 2006. Integrated regional changes in arctic climate feedbacks: implications for the global climate system. *Annual Rev. Environmental Resources*, **31**, 61-91.

McGuire, A.D., Anderson, L., Christensen, T.R., Dallimore, S., Guo, L.D., Hayes, D., Heimann, M., Macdonald, R. and Roulet, N. 2009. Sensitivity of the carbon cycle in the Arctic to climate change (Review). *Ecological Monographs*, **79**(4), 523-555.

Mehrbach, C., Culberson, C.H., Hawley, J.E., and Pytkowicz, R.M., 1973. Measurement of the apparent dissociation constants of carbonic acid in seawater at atmospheric pressure. *Limnology and Oceanography*, **18**, 897–907.

Millero, F. J., 2007. The Marine Inorganic Carbon Cycle. *Chemical Reviews*, **107**(2), 308–341.

Moore, E.E., Gremeier, J.M., and Davis, J.R., 2003. Gray whale distribution relative to forage habitat in the northern Bering Sea: Current conditions and retrospective summary. *Canadian Journal of Zoology*, **81**, 734–742.

Moran, S.B., Kelly, R.P., Hagstrom, K., Smith, J.N., Grebmeier, J.M., Cooper, L.W., Cota, G.F., Walsh, J.J., Bates, N.R., Hansell, D.A., Maslowski, W., Nelson, R.P., and Mulsow, S., 2005. Seasonal changes in POC export flux in the Chukchi Sea and implications for water column-benthic coupling in Arctic shelves. *Deep-Sea Research,* **52** (22-24), 3427-3451, doi:10.1016/j.dsr2.2005.09.011.

Murata, A., and Takizawa, T., 2003. Summertime carbon dioxide sinks in shelf and slope waters of the western Arctic Ocean. *Continental Shelf Research*, **23**(8), 753-776.

Omar, A.M., Johannessen, T., Olsen, A., Kaltin, S., and Rey, F., 2007. Seasonal and interannual

variability of the air-sea carbon dioxide flux in the Atlantic sector of the Barents Sea. *Marine Chemistry*, **104**, 203–213, doi:10.1016/j.marchem.2006.11.002.

Orr, J.C., Fabry, V.J., Aumont, O., Bopp, L., Doney, S.C., Feely, R.A., Gnanadesikan, A., Gruber, N., Ishida, A., Joos, F., Key, R.M., Lindsay, K., Maier-Reimer, E., Matear, R., Monfray, P., Mouchet, A., Najjar, R.G., Plattner, G.K., Rodgers, K. B., Sabine, C.L., Sarmiento, J.L., Schlitzer, R., Slater, R.D., Totterdell, I J., Weirig, M.F., Yamanaka, Y., and Yool, A., 2005. Anthropogenic ocean acidification over the twenty-first century and its impact on calcifying organisms. *Nature*, **437**(7059), 681–686.

Overland, J.E., and Stabeno, P.J., 2004. Is the climate of the Bering Sea warming and affecting the ecosystem? *Eos, Transactions of the American Geophysical Union*, **85**(33), 309, doi:10.1029/2004EO330001.

Pipko, I.I., Semiletov, I.P., Tishchenko, P.Y., Pugach, S.P., and Savel'eva, N.I., 2008. Variability of the carbonate system parameters in the coast-shelf zone of the East Siberian Sea during the autumn season. *Oceanology*, **48**(1), 54-67.

Raymond, P.A., McClelland, J.W., Holmes, R.M., Zhulidov, A.V., Mull, K., Peterson, B.J., Striegl, R.G., Aiken, G.R., and Gurtovaya, T.Y., 2007. Flux and age of dissolved organic carbon exported to the Arctic Ocean: A carbon isotopic study of the five largest arctic rivers, *Global Biogeochemical Cycles,* **21**(4), doi:10.1029/2007GB002934.

Rachold, V., Eicken, H., Gordeev, V.V., Grigoriev, M.N., Hubberten, H.-W., Lisitzin, A.P., Shevchenko, V.P., and Schirmeister, L., 2004. Modern terrigenous organic carbon input to the Arctic Ocean. in *The Organic Carbon Cycle in the Arctic Ocean*, edited by R.S. Stein and R.W. Macdonald, pp. 33–69, Springer, New York.

Roach A.T., Aagaard, K., Pease, C.H., Salo, S.A., Weingartner, T.J., Pavlov, V., and Kulakov, M., 1995. Direct measurements of transport and water properties through Bering Strait. *Journal of Geophysical Research*, **100**(C9), 18,443–18,457.

Sabine, C.L. and Feely, R A., 2007. The oceanic sink for carbon dioxide. In D. Reay, N. Hewitt, J. Grace and K. Smith, Eds. *Greenhouse Gas Sinks*. pp. 31–49. CABI Publishing, Oxfordshire, UK.

Sabine, C.L., Feely, R.A., Gruber, N., Key, R. M., Lee, K., Bullister, J.L., Wanninkhof, R., Wong, C.S., Wallace, D.W.R., Tilbrook, B., Millero, F. J., Peng, T.-H., Kozyr, A., Ono, T., and Rios, A.F., 2004. The Oceanic Sink for Anthropogenic CO_2. *Science*, **305**(5682), 367–371.

Semiletov, I.P., 1999. Aquatic sources of CO_2 and CH_4 in the Polar regions. *Journal of Atmospheric Sciences*, **56**(2), 286-306.

Springer, A.M., McRoy, C.P., and Flint, M.V., 1996. The Bering Sea Green Belt: shelf-edge processes and ecosystem production. *Fisheries Oceanography*, **5**(3-4), 205–223.

Steinacher, M., Joos, F., Frolicher, T.L., Plattner, G.-K., and Doney, S.C., 2009. Imminent ocean acidification of the Arctic projected with the NCAR global coupled carbon-cycle climate model. *Biogeosciences***, 6**, 515-533.

Wang, W.Q., Yang, X.T., Huang, H.B., and Chen, L.Q., 2003. Investigation on distribution and fluxes of sea–air CO_2 of the expedition areas in the Arctic Ocean. *Science in China Series D—Earth Sciences*, **46**, 569–580.

Weiss, R.F., 1974. Carbon dioxide in water and seawater: The solubility of a non-ideal gas. *Marine Chemistry*, **2**, 203–215.

Woodgate, R.A., Aagaard, K., and Weingartner, T.J., 2005. Monthly temperature, salinity and

transport variability of the Bering Strait through flow. *Geophysical Research Letters*, **32** (4), L04601, doi:10.1029/2004GL021880.

Yamamoto-Kawai, M., McLaughlin, F.A., Carmack, E.C., Nishino, S., and Shimada, K., 2009. Aragonite undersaturation in the Arctic Ocean: effects of ocean acidification and sea ice melt. *Science,* **326**(5956), 1098-1100, doi: 10.1126/science.1174190.

Zachos, J.C., Röhl, U., Schellenberg, S.A., Sluijs, A., Hodell, D.A., Kelly, D.C., Thomas, E., Nicolo, M., Raffi, I., Lourens, L.J., McCarren, H., Kroon, D., 2005. Rapid Acidification of the Ocean During the Paleocene-Eocene Thermal Maximum. Science, Vol. 308. no. 5728, pp. 1611 – 1615.